Title

A PARTIAL WAVE ANALYSIS OP THE REACTION nN->nnN in the c.m. ENERGY RANGE 1300 - 2000 MeV

Authors

Herndon, D.J.
Longacre, R.
Miller, L.R.
et al.

Publication Date

1972-08-01

Presented at XVIth International Conference on High Energy Physics, Chicago, IL, September 6-13, 1972

LBL-1065
SLAC-PUB-1108

A PARTIAL WAVE ANALYSIS OF THE REACTION $\pi N \to \pi\pi N$ in the c.m. ENERGY RANGE 1300 - 2000 MeV

D. J. Herndon, R. Longacre, L. R. Miller, A. H. Rosenfeld, G. Smadja, P. Soding, R. J. Cashmore and D.W.G.S. Leith

August 25, 1972

Prepared for the U.S. Atomic Energy Commission under Contract W-7405-ENG-48

DISCLAIMER

LBL-1065
SLAC-PUB-1108

A Partial Wave Analysis of the Reaction $\pi N \to \pi\pi N$ in the c.m. Energy Range 1300 - 2000 MeV*

D.J. Herndon, R. Longacre+, L.R. Miller,
A.H. Rosenfeld, G. Smadja, and P. Soding**
Lawrence Berkeley Laboratory
University of California, Berkeley, California 94720

R.J. Cashmore and D.W.G.S. Leith
Stanford Linear Accelerator Center
Stanford University, Stanford, California 94305

25 August 1972

Abstract

A continuous set of partial wave amplitudes (in the c.m. energy range 1300 - 2000 MeV) is presented. A D13 (~ 1700) state is observed in two channels, the existence of a P13 (~ 1800) is corroborated, but there is little evidence for a P33 (1700). The presence of many resonances in the channels $N\rho$ and $N\sigma$ are observed, supplementing the information on their $\pi\Delta$ decays.

Submitted to XVIth International Conference
on High Energy Physics, Chicago, September, 1972
to be presented by G. Smadja

---

*Work supported by the U.S. Atomic Energy Commission
**Present address, DESY, Notkestieg 1, 2000 Hamburg-52

+Fellow of the Miller Institute for Basic Research in Science, on leave of absence from C.E.N. Saclay (France)

1. Introduction

Elastic phase shift analysis has provided us with an impressive list of resonances, which is both the essence of our understanding of baryon spectroscopy and also the main testing ground for many of the ideas on the dynamics of hadronic processes. The agreement between the many independent groups is very impressive,[1,2] and gives confidence in the resulting scattering amplitudes.

Corresponding investigation of the inelastic scattering reactions has not kept pace with the elastic investigations. This derives not only from the lack of data (with high statistics, and systematically spread in energy) but also from the complexity of the phenomenological analysis. However, the study merits the effort. The inelastic cross section represents a very substantial fraction of the total πN cross section, even at 1.0 GeV/c, and it is therefore intrinsically interesting to understand the scattering process. In addition, the inelastic decays of N^* are a very specific signature of the state and its properties, and therefore an important study in their own right. Finally, for resonances with very small coupling to the elastic channel, these studies are the only means of investigating the resonance in a formation experiment.

In the resonance region the principle inelastic reaction is

$$\pi N \rightarrow \pi\pi N \qquad (1)$$

We have therefore made a detailed study of this channel in the c.m. energy range 1.3 - 2.0 GeV.

In previous analyses of reaction (1) two approaches have been taken:

(a) selection of sub samples of the data to isolate specific reactions[3] e.g., $\pi N \rightarrow \pi\Delta$

(b) the use of an isobar model in an effort to fit the whole reaction taking into account the effects due to strongly overlapping resonances in the final state[4,5,6]

We have developed the second of these approaches by including many more

intermediate states and using the maximum likelihood technique in confronting the data with theory. These developments have enabled us to produce a continuour solution from energy independent fits throughout the energy range we consider.

2. The Data

The data used in this work have been gathered from several bubble chamber experiments listed in Table I, together with their statistics. The sample of events thus obtained covers the reactions:

$$\pi^- p \to p\pi^o,\ \pi^- p \to n\pi^+\pi^-,\ \pi^+ p \to p\pi^+\pi^o,\ \pi^+ p \to n\pi^+\pi^+$$

at center of mass energies between 1.3 and 2 GeV. The biases and inefficiencies for these final states have been discussed by the authors.[4,5,6,7,8] As they are small, we did not correct for such losses in the subsequent analysis.

We show in Fig. 1 a set of Dalitz plots for these reactions: they all have strong bands associated with Δ or ρ production which suggests the use of an isobar model. Furthermore, we see in Fig. 2 that the distribution of θ, the scattering angle of the final nucleon has a complicated structure, rapidly changing with energy. We can therefore anticipate that many partial waves will be necessary, with fast variations of their moduli and phases. This observation is consistent with the presence of resonance-like structure in the inelastic cross sections shown in Fig. 3.

3. The Model

In order to analyze the reaction we have used an extended isobar model.[9] This contains the following assumptions.

(1) The reaction is considered as the superposition of several quasi two body reactions. Only $\pi\Delta(1236)$, $N\rho(760)$ and $N\sigma$ are used as intermediate states. The first two of these are clearly present

in the data and it is well known[10] that the I=0, J=0 $\pi\pi$ interaction is strong in the mass regions we consider.

(2) Each intermediate state can proceed through a number of partial waves. We only consider waves in which the final orbital angular momentum is less than 3. These waves are listed in Table II and the notation summarized in Fig. 4.

(3) The amplitude for the reaction to proceed through a particular intermediate state α is written as

$$T_\alpha = A_\alpha \, K(\alpha) \, G(\alpha) \tag{1.1}$$

where

$K(\alpha)$ contains all the kimematical information related to the angular momentum decomposition of the production reaction. In particular, it contains a centrifugal barrier factor Q^L where Q is the momentum and L the orbital angular momentum in the intermediate state.[11]

$G(\alpha)$ represents the final state interaction and is introduced using the Watson Final State Interaction theorem[12]

$$G(\alpha) = \frac{e^{i\delta_\alpha} \sin \delta_\alpha}{q^{\ell_\alpha + 1}}$$

Here δ_α is the appropriate elastic phase shift for the strongly interacting pair of particles (e.g., the πN in the $\Delta(1236)$).

Each A_α is then expected to be a slowly varying function of the subsystem mass and we therefore approximate it by a constant at each individual c.m. energy. This is the partial wave amplitude.

(4) The quasi-two body amplitudes can be added. This implies some double counting but it can be shown to be small.[13]

This construction of the scattering amplitude allows easy fitting to all single pion production channels and hence to the isospin decomposition of the scattering amplitude.

There are, however, some limitations which must be observed.

(i) The final state factors and centrifugal barriers are not uniquely defined. They could be multiplied by slowly varying functions, but we have checked that we are largely insensitive to such changes.

(ii) We do not allow for $\pi N^*_{\frac{3}{2}}$ intermediate states but these do not seem to be important in the channels we analyze.

(iii) No direct 3 particle decays are considered. The slowly varying 'σ' may, however, partially represent such a process.

4. The Likelihood Fitting

The definition of an $N\pi\pi$ event at a given energy requires 4 quantities. In order to exploit all of the correlations between these quantities we have used the maximum likelihood method in fitting the data.

Let $p_c(i, \vec{A})$ be the probability density for event i in channel c as a function of the partial wave amplitudes $\vec{A}$ [eq. (1.1) of the previous section]. p_c is normalized so that the integration over phase space gives unity. For one channel c, the likelihood L_c is given by

$$\log (L_c) = \sum_{i=1}^{N_c} \left[\log p_c(i, \vec{A})\right]$$

where the summation runs over all events in that channel. When dealing with several channels the probability density for an event is the product of the probability for it being found in channel c and the probability for it having a particular kinematical configuration within that channel.

Furthermore, we use data in which the no. of events/μb is not always the same in each channel (the data come from many experiments). If we define quantities $L_c = \frac{N_c}{\sigma_c(\text{obs})}$ then we can write the probability that an event is found in a particular channel as

$$\frac{\sigma_c(\vec{A})L_c}{\sum_c \sigma_x(\vec{A})L_x}$$

and the resulting likelihood function becomes

$$\log L = \sum_c \sum_{i=1}^{N_c} \log\left[\left(\frac{\sigma_c(\vec{A})L_c}{\Sigma_x \sigma_x(\vec{A})L_x}\right) p_c(i, \vec{A})\right]$$

$$= \sum_c N_c \log\left(\frac{\sigma_c(\vec{A})L_c}{\Sigma_x \sigma_x(\vec{A})L_x}\right) + \sum_c \sum_{i=1}^{N_c} \log p_c(i, \vec{A})$$

where $\sigma_c(\vec{A})$ is the calculated channel cross section. The contribution of the first term to the likelihood is a maximum when the calculated channel cross sections correspond to the observed cross sections.[14] The fitting program was capable of using as many as 60 partial waves.[15]

5. The Fitting Procedure

The number of events used in the analysis are given in Table III. They were binned into energy intervals of 30 to 40 MeV, the central value varying by steps of 30 to 40 MeV also, except between 1540 and 1650 MeV, where no data were available.

In this section, we now give an outline of the procedure we have followed in arriving at our final solution. This procedure involves a number of distinct stages.

(i) Generation of Starting Values and Initial Maximization at Each Energy (SEEK)

(a) Initially we begin with our complete set of 60 partial waves given in Table I.

(b) We generate ~ 2000 random sets of partial-wave amplitudes, calculate a likelihood for each, and retain the 6 highest.

(c) These 6 sets are then used as initial values in the maximization program leading to 1-6 final maxima (some of the initial solutions converge to the same final solution).

(ii) Removal of Unnecessary Waves

(a) We look at all solutions at all energies and remove waves (from all amplitude sets) which are "small" (within 2 standard deviations of zero) at 3 or more energies.

(b) Re-maximize at each energy with this smaller set of amplitudes starting from the final parameter values of (ic) (or of (iib) in the iteration procedure).

(c) Iterate (iia) and (iib) until we obtain a final irreducible set of waves.

At this stage, usually about 3 solutions remain at each energy (for $E < 1540$, we have only one).

(iii) Consistency with Elastic Phase Shift Analyses (EPSA)

There is a danger in (iia) that we will remove waves which become necessary at our highest energies (e.g., F37 waves). In order to identify this we compare our cross section predictions with those of EPSA. Wherever there is disagreement in a particular incoming partial wave we add appropriate amplitudes to the final set of (iic) and re-maximize. In this manner we reintroduce necessary waves which have been lost in Stage (ii).

(iv) Continuity

(a) From the solutions we have attempted to define continuous chains. This has been done in two ways

(i) The parameter values of each solution at a given energy were used as starting values (for the maximization process) at the adjacent energy points. In the majority (~ 75%) of cases these starting values led to already existing solutions.

(ii) Among solutions which were qualitatively similar, we kept the one that was most satisfactory with respect to criteria of continuity and likelihood.

(b) When we obtained continuous chains in most waves, some waves (e.g., ρ_3 DD15, $\pi\Delta$ DD35) were observed to possess discontinuous behavior in the Argand diagram, i.e., they showed 180° phase changes between adjacent energies. We first examined these cases to see if the discontinuities could be attributed to local maxima. We did not find this to be the case and these waves were removed and all the solutions remaximized.

(v) Final Solution

In summary we find one final solution which possesses all the following properties:

(i) At each energy the solution parameters correspond to a maximum in the likelihood function and have a high likelihood (usually the highest of the competing solutions).

(ii) The solution at each energy propagates to the solution at the adjacent energies above and below.

(iii) Qualitatively it has no discontinuous motion between adjacent energies.

(iv) It possesses good agreement with the EPSA predictions for inelastic cross sections.

The initial set of waves used is given in Table II together with the final 24 remaining at our highest energy (only 10 waves are needed around 1400 MeV).

(vi) Uniqueness and Stability of the Solutions

The crucial step was the selection of a good subset of waves. For this subset, we have found only one solution which satisfies all the requirements listed in (v), and we thus believe that the larger waves are uniquely determined. We attempted fits where one of these waves was replaced by another one with the same J^P, but the likelihood dropped dramatically. We cannot be as certain in the case of smaller waves, the amplitudes of which are never more than 2 or 3 standard deviations from zero. Furthermore, as we have rather large energy steps, our emphasis on continuity clearly biases us against very narrow resonances.

6. Quality of the Fits

In order to evaluate the quality of the fits we have studied the following:

(a) Description of the data using the partial wave amplitudes

In Figs. 1 and 2 we presented the data at 1.7 GeV together with the results of the fit. The agreement is excellent, the major correlations being well reproduced. However, at our higher energies two effects are noticeable.

(i) the ρ and Δ mass peaks are slightly shifted (Fig. 1). This may be a result of assuming that the partial wave amplitudes A_α are independent of subsystem masses.

(ii) the nucleon scattering angle (Fig. 2) demonstrates the onset of peripherality which has not been entirely reproduced by the ρ and σ partial waves allowed within the model at present.

(b) Agreement with Elastic Phase Shift Analyses

Elastic phase shift analyses (EPSA) provide an upper bound for the inelastic cross section in each incoming partial wave (IJ^P). Our results, as shown in Fig. 5, always satisfy this requirement within errors, while at low energies we saturate the EPSA bound as expected.

(c) Cross Section for $\pi^- p \to n\pi^o\pi^o$

This channel is not included in the fitting process as no bubble chamber events are available. However, we can compare our predicted cross section for this process with the observed values and we do indeed find good agreement as shown in Fig. 6.

7. The Partial Wave Amplitudes

At each energy the solution of any fits to inelastic reactions are only defined up to an arbitrary phase. Thus in order to give Argand diagrams of the partial wave amplitudes we must determine the absolute phase of the set of amplitudes at each energy. This has been done by performing a multi-channel K-matrix fit both to the published elastic and to our inelastic transition amplitudes in specific partial waves at energies where a prominent resonance dominates. These fits are described in Section 8.

The Argand diagrams for both elastic and inelastic scattering amplitudes are displayed in Fig. 5. In Table Iv we give a summary of the major characteristics of each partial wave together with the comments on the resonance

interpretations that occur. We leave a discussion of the implications until the next section.

8. Discussion of Results

The agreement with the data and EPSA together with the continuity of the solution are impressive even though there are some discrepancies at the higher energies. Resonant structure is a strong feature of all 3 channels, $\pi\Delta$, $N\rho$, $N\sigma$. We can make the following points concerning our results:

(a) Resonances

(i) We observe unambiguously a D13 resonance in the region of 1700 MeV, a state predicted by the L excitation symmetric quark model.[17]

(ii) There is no evidence for a strong P33 resonance at ~ 1700 MeV even though the $\pi\Delta$ cross section is large in this wave. This is reminiscent of the behavior of the PP13 $K\Delta$ wave in K^+p scattering.[18] This observation also casts doubt on the identification of the P11 (1470) and a P33 (1700) with the first radial excitation of the P11 (930) and P33 (1236) in the symmetric quark model.[17]

(iii) The existence of a P13 (1860) is strengthened by our analysis, the $N\rho$ channel being the dominant decay mode.

(iv) The $N\rho$ system is a major decay channel for the D13 (1520), F15 (1680), P13 (1860), F35 (1890), and F32 (1950).

(v) The $\pi\Delta$ decay amplitudes of the F15 (1680) and D15 (1670) are in close agreement with Solution A of our previous analysis,[3] where we made a Δ^- cut and fit to the reaction $\pi^-p \to \Delta^-\pi^+$.

(vi) It is possible to extract individual channel cross sections into $\pi\Delta$, $N\rho$, and $N\sigma$. Fig. 6 contains these partial cross sections. At low energies the sum is much larger than the total inelastic cross section due to the presence of strong destructive interferences.

(b) Discrepancies

(i) Unfortunately our fits do not give very satisfactory predictions for the $\pi^+\pi^+n$ cross sections at higher energies, falling short by approximately 3 mb. This problem, or shortcoming of the model, may be attributed to the fact that we include only I = 3/2 isobar formation, whereas the data (for this channel only) show very clear evidence of I = 1/2 isobar formation. (Both N*(1530) and N*(1690) are observed in $n\pi^+$ mass spectra). The $N^*_{\frac{1}{2}}$ isobars do not seem to be present in the other channels.

(ii) Our solutions do not require any waves derived from an incident D35 state and we thus fall dramatically short of the EPSA predictions. We also observe that the F37 inelastic cross section is not saturated. However, it is interesting to note that the sum of these discrepancies corresponds approximately to the $\pi^+\pi^+\pi^-p$ (~ 5 mb at 1925 MeV) and unaccounted $\pi^+\pi^+n$ (~ 3 mb) cross sections.

(iii) The observation of the excess of events for small nucleon scattering angles suggests, as an improvement, the inclusion of the high angular momentum waves derived from π exchange.

9. The K-Matrix Parameterization

(a) Formalism

As mentioned earlier, our inelastic amplitudes found at each energy are known only up to an overall phase, so that we cannot even check continuity in energy. We next want to tie them all together in a smooth, energy-dependent fit, and at the same time relate them to the known elastic amplitudes. To do this we use a K-matrix, so that the resulting T-Matrix will automatically satisfy unitarity.

Our K-matrix is a sum of factorizable poles $\frac{\gamma^\alpha \gamma^\beta}{S_r - S}$ for up to two

resonances (r = 1, 2) plus a constant background $k_o^{\alpha\beta}$. We use a reduced k-matrix:

$$k^{\alpha\beta} = \sum_{r=1}^{2} \frac{\gamma_r^\alpha \gamma_r^\beta}{S_r - S} + k_o^{\alpha\beta}.$$

Such a form, factorizable at each pole, guarantees that for each K-matrix pole we shall find <u>one</u> nearby T-matrix pole.

To express the T matrix in terms of $k^{\alpha\beta}$ we first define a reduced T-matrix $t^{\alpha\beta}$ given by

$$T^{\alpha\beta} = t^{\alpha\beta}\, f(\alpha)\, f^*(\beta)$$

where $f(\alpha)$ are the kinematic factors of Eq. (1.1). We then have the standard relation between t- and k- matrices

$$t\,[1 - \tfrac{1}{2}\, i\, t\, Q\, k] = k$$

where Q is a nearly-diagonal* momentum matrix

$$Q^{\alpha\beta} = \delta^{\alpha\beta}\, \frac{\bar{Q}^\alpha}{4\, S}$$

For a two particle state, $\bar{Q}_\alpha$ is the center of mass momentum, and for a three-particle state

$$\bar{Q}_\alpha = \int f(\alpha) f^*(\alpha) Q^\alpha\, \frac{q^\alpha}{4\, S_\alpha}\, dS_\alpha$$

is the average momentum of the subsystem produced in wave α.

(b) Fits

We fit k_o and γ_α^r to t^{11} (known from EPSA) and $t^{1\alpha}$ (given by our analysis). In each IJ^P subspace, our k matrix couples up to 7 channels, namely 1 elastic and 6 inelastic states $\pi\Delta$ and $N\rho_3$ (each with possibly

---

*More precisely, Q is not a diagonal matrix when proper account is taken of the interferences between the different pairs of particles in the final state. This effect was included in our treatment, and will be described in the thesis of Ronald Longacre.(21)

two waves like DS13 and DD13), $N\rho_1$, $N\sigma$. As an example, we detail the parameters involved for D13: we have 5 channels:

1: πN (D13)

2: $\pi\Delta$ (DS13)

3: $\pi\Delta$ (DD13)

4: $N\rho_3$(DS13)

5: $N\sigma$ (DS13)

which implies 15 parameters for k^o, 5 coupling constants for each of 2 resonance, and two corresponding pole positions.

i.e., a total of 27 parameters. The fit is performed over an energy range of 1310 to 1810 MeV where 150 data points are available.

Wherever we have made these fits the results are included in the Argand diagrams in Fig. 5. The qualitative agreement is excellent, particularly as we have used a rather modest number of parameters. In Table V we summarize the pole positions of the K-matrix although these will differ from the real part of the pole in the T-matrix. The interpretation of the coupling constants is not clear and we postpone a discussion of this point until later publications.

10. Conclusions

The elastic phase shift analyses only relate to one aspect of the πN interaction and the analysis described here represents a substantial progress in providing complimentary information on the inelastic channels.

We have strong evidence for the existence of a resonance in D13 at 1700 MeV. While this has been suggested in previous EPSA and photoproduction experiments[20] the most recent EPSA[2] finds no evidence for it at current sensitivity. Such a state has long been required by the quark model[17]. Furthermore, we have strengthened the interpretation of many other resonances while casting serious doubt on the existence of a P33 state at ~ 1700 MeV.

The first reliable determination of σN and ρN partial wave amplitudes has indicated the appearance of many resonances in this channel. These together with our improved knowledge of the $\pi\Delta$ system begin to allow a complete picture of the πN inelastic reactions.

Finally, we are at present using these amplitudes to study resonance parameters and coupling and their relation to other theories of hadron interactions.

Acknowledgments

We wish to thank the Oxford, U.C. Riverside, and Saclay groups, especially A. Jones, D. Saxon (Oxford), S-Y Fung, A. Kernan (U.C.R.), B. Deler, Nguyen Thuc Diem, J. Dolbeau (Saclay), W. Michael, G. Kalmus (LBL), for use of their data in this analysis. We also thank J.P. Berge, A.D. Brody, B. Deler, A. Kernan, B. Levi, L.R. Price, and B. Shen for their contributions to the early phase of the experiment.

References

1. R. Ayed, et al., Phys. Letters 31B, 598 (1970)
2. S. Almehed, et al., Nucl. Phys. B40, 157 (1972)
3. A.D. Brody, et al., Phys. Letters 34B, 665 (1971); U. Meheani et al., UCR 34 P107 B-146. "A Partial Wave Analysis of $\pi^+ p \rightarrow \pi^o \Delta^{++}$ from (1820-2090) MeV." The data from this experiment has been included in our analysis.
4. M. DeBeer, et al., Nucl. Phys. B12, 599 and 617 (1969); further analyses may be found in the theses of B. Deler (CEA-R-3579, 1969), G. Smadja (Orsay Series A, No. 556, 1969) and in the forthcoming theses of Nguyen Thuc Diem and Jean Dolbeau.
5. M. G. Bowler, et al., Nucl. Phys. B17, 331 (1970)
6. W. Chinowsky, et al., Phys. Rev. D2, 1790 (1970)
7. A. D. Brody, et al., Phys. Rev. D4, 2693 (1971)
8. A. Kernan, et al., data unpublished at present
9. B. Deler, et al., Nuovo Cimento 45A, 559 (1966)
10. J. P. Baton, et al., Phys. Rev. 176, 1574 (1968)
11. J. M. Blatt and V. F. Weisskopf, Theoretical Nuclear Physics (John Wiley and Sons, Inc., New York, 1956)
12. K. M. Watson, Phys. Rev. 88, 1163 (1952)
13. G. Smadja, LBL - 382 (unpublished)
14. F. T. Solmitz, Annual Rev. of Nucl. Sci. 14, 375 (1964)
15. L. R. Miller, LBL - 38 (unpublished)
16. C. B. Chiu, et al., Phys. Rev. 156, 1415 (1967)
    F. Bulos, et al., Phys. Rev. 187, 1827 (1969)
    B. C. Barish, et al., Phys. Rev. 135B, 1416 (1964)
17. R. Dalitz, in Pion-Nucleon Scattering, ed., Shaw and Wong (John Wiley and Sons, Inc., New York, 1969)
    O. Greenberg, Proc. Lund Conf., 1969, p. 398
    R. Feynman, et al., Phys. Rev. D2, 1267 (1970)
18. R. G. Bland, et al., Nucl. Phys. B13, 595 (1969)

19. A. Donnachie, et al., Phys. Rev. Letters 26B, 161 (1968)

P. Bareyre, et al., Phys. Rev. 165, 1730 (1968)

20. S. R. Deans, et al., Phys. Rev. Letters 28, 1739 (1972)

21. Ronald Longacre, LBL 938 (thesis).

Table I

Experiments used in this analysis

Laboratory (Reference)	Energy Range $\sqrt{s}$ (GeV)	Number of Events $\pi^+\pi^-n$	$\pi^-\pi^0p$
SLAC-LBL (7)	1.47 → 1.50	1010	648
	1.65 → 1.97	41175	27946
Oxford (6)	1.31 → 1.54	18502	5892
Saclay (4)	1.39 → 1.53	13340	7314
Total	1.31 → 1.97	74027	41800

Laboratory (Reference)	Energy Range	$\pi^+\pi^0p$	$\pi^+\pi^+n$
Oxford (5)	1.43 → 1.56	7262	1374
Riverside-LBL (8)	1.82 → 2.09	41412	17255
Saclay (4)	1.64 → 1.97	11522	3382
Total	1.43 → 2.09	60196	22011

Table II

The 60 waves possible with angular momenta L, L', ℓ each ≤ 3. There are two nucleon-rho terms in the isobar model, indicated by ρ_3 and ρ_1, where the subscript indicates the coupling between the spin of the ρ ($\ell = 1$) and the spin of the outgoing nucleon. The boxes indicate the final subset of waves used in our fits.

Incident Wave	$\pi\Delta$	$N\rho_3$	$N\rho_1$	$N\sigma$
S11	SD11	SD11	**SS11**	**SP11**
P11	**PP11**	PP11	PP11	**PS11**
D13	**DS13**	**DS13**	----	**DP13**
	DD13	DD13	DD13	L'>3
P13	PP13	PP13	**PP13**	PD13
	PF13	PF13	----	----
D15	**DD15**	DD15	DD15	DF15
F15	**FP15**	**FP15**	----	**FD15**
	FF15	FF15	FF15	----
F17	FF17	FF17	FF17	(L'>3)
S31	**SD31**	SD31	**SS31**	
P31	**PP31**	PP31	**PP31**	
D33	**DS33**	**DS33**	----	
	DD33	DD33	DD33	
P33	**PP33**	PP33	PP33	
	PF33	PF33	----	
D35	DD35	DD35	DD35	
F35	FP35	**FP35**	----	
	FF35	FF35	FF35	
F37	**FF37**	**FF37**	FF37	

Table III

Number of Events for the Energy Bins Used in the Fits

C.O.M. Energy	Range (MeV)	$\pi^- p \to \pi^+ \pi^- n$	$\pi^- p \to \pi^- \pi^o p$	$\pi^+ p \to \pi^+ \pi^o p$
1310	1300 - 1330	1069	151	
1340	1330 - 1360	1664	11	
1370	1360 - 1380	2471	2	
1400	1380 - 1410	5049	964	78
1440	1430 - 1460	4918	1802	359
1470	1460 - 1480	3252	1629	175
1490	1480 - 1510	5555	3197	1523
1520	1510 - 1530	3241	2588	795
1540	1530 - 1560	3905	3285	1114
1650	1630 - 1670	6061	3757	2467
1690	1670 - 1710	5901	3689	1139
1730	1710 - 1750	3455	2630	4061
1770	1750 - 1790	3214	2352	2853
1810	1790 - 1830	2447	1541	3855
1850	1380 - 1870	3931	3183	6372
1890	1870 - 1910	5072	3170	12690
1930	1910 - 1950	5817	4080	4298
1970	1950 - 1990	5277	3544	7744
Total	1300 - 1990	72299	41575	49523

Table IV

Partial Wave	EPSA Results	Discussion of cm results	Decay channels and general comments on our results
S11	M = 1535 $X_{inel} \sim 0.65$	Not observed in our data; this is consistent with a large branching fraction (~0.55) into ηN	πN, ηN
	M = 1700 $X_{inel} \sim 0.35$	Resonant loops are clearly present in the σN and ρN channels. No evidence of coupling to $\pi\Delta$	πN, σN, ρN
	M ~ 2100 $X_{inel} \sim 0.5$	Not sensitive to this state, since it is at the edge of our energy range	πN
P11	M ~ 1470 $X_{inel} \sim 0.4$	Clear resonance behavior in $\pi\Delta$ and $N\sigma$ channels	πN, $\pi\Delta$, σN
	M ~ 1780 $X_{inel} \sim 0.7$	Again both $\pi\Delta$ and $N\sigma$ channels exhibit resonant loops	πN, $\pi\Delta$, σN
P13	M = 1860 $X_{inel} \sim 0.75$	Clear resonant behavior is observed in the ρN channel	πN, ρN Strengthens the observation in EPSA
D13	M ~ 1520 $X_{inel} \sim 0.4$	Strong resonant behavior in the $N\rho$ and $\pi\Delta$ channels (even though $N\rho$ is 300 MeV below threshold).	πN, ρN, $\pi\Delta$
	Suggestion of resonance with M ~ 1750 MeV. No information on inelasticity.	Clear resonant motion in σN and $\pi\Delta$	πN, σN, $\pi\Delta$ First unambiguous observation of resonant behavior in this region.
D15	M = 1670 $X_{inel} \sim 0.58$	The $\pi\Delta$ channels show strong resonant behavior, saturating the unitary bound near the accepted resonant mass	πN, $\pi\Delta$
F15	M = 1688 $X_{inel} \sim 0.38$	This resonance is observed in σN, ρN, and $\pi\Delta$ with comparable strength.	πN, σN, ρN, $\pi\Delta$

Partial Wave	EPSA Results	Discussion of cm results	Decay channels and general comments on our results
S31	M = 1650 $X_{inel} \sim 0.72$	We unfortunately lack the experimental data which would reveal the behavior of this wave in the resonance region. The present points above 1650 show a smooth behavior which is compatible with the accepted resonance mass.	πN, $\pi\Delta$
P31	Suggestion of resonance with M ~ 1910 MeV. $X_{inel} \sim 0.7$ (poorly determined)	Weak evidence for resonant behavior in the $\pi\Delta$ channel	πN, $\pi\Delta$
P33	Suggestion of resonance with M ~ 1670 MeV. $X_{inel} \sim 0.90$ (poorly determined)	No evidence for resonant behavior in any channel	πN Resonance existence is unlikely
D33	M ~ 1670 $X_{inel} \sim 0.85$	Our analysis is consistent with a resonance interpretation for the $\pi\Delta$ channel	πN, $\pi\Delta$
F35	M ~ 1890 $X_{inel} \sim 0.83$	Strong resonance behavior seen in ρN channel	πN, ρN
F37	M = 1950 $X_{inel} \sim .55$	Clear resonance behavior is apparent in ρN and $\pi\Delta$ channels	πN, ρN, $\pi\Delta$

TABLE V

Resonance Pole Positions in K-matrix Fits

Wave	P 11	P 13	D 13	D 15	F 15	F 35	F 37
Pole Position MeV	1497 1801	1754	1520 1733	1685	1682	1933	1930

Figure Captions

Fig. 1: Dalitz plots for the 3 final states $\pi^+\pi^-n$ (1.1), $\pi^-\pi^op$ (1.2), $\pi^+\pi^op$ (1.3) at four center of mass energies: 1490, 1650, 1770, 1930 MeV. The side of the little squares is proportional to the predicted density of our fits. On the projected distributions, the dotted line is the experimental data, while the solid histogram is the result of the fit.

Fig. 2: Distribution of the angle of the final nucleon with respect to the incident pion in the center of mass. The histograms are given at four center of mass energies: 1490, 1650, 1770, 1930 MeV for the same channels as in Fig. 1. The dotted line is the data, the solid histogram the result of the fit.

Fig. 3: Cross sections as a function of center of mass energy for the four channels $\pi^o\pi^on$, $\pi^+\pi^-n$, $\pi^-\pi^op$, $\pi^+\pi^op$. The dots $\dashv$ are the experimental values with their error bars. The crosses correspond to the numbers found in the fit.

Fig. 4: Schematic representation of the isobar model and definition of the partial wave notation.

Fig. 5: Argand diagrams and partial wave cross sections for the elastic and inelastic channels. The smooth curve on the Argand diagrams is the amplitude obtained from the K matrix when the description was possible. Cross hatched marks on the curve correspond to the energies D, E, F etc. The arrows indicate the known resonances of Table V. The total inelastic contribution in each elastic wave $\dashv$ is compared with the sum of the inelastic contributions we observe. Facing each inelastic Argand diagram, we give the variation with energy of the square modulus of the wave.

Fig. 6: Cross sections for $\pi N \rightarrow \Delta\pi$, ρN, σN as a function of the center of mass energy. The statistical error bars are given at 3 energies.

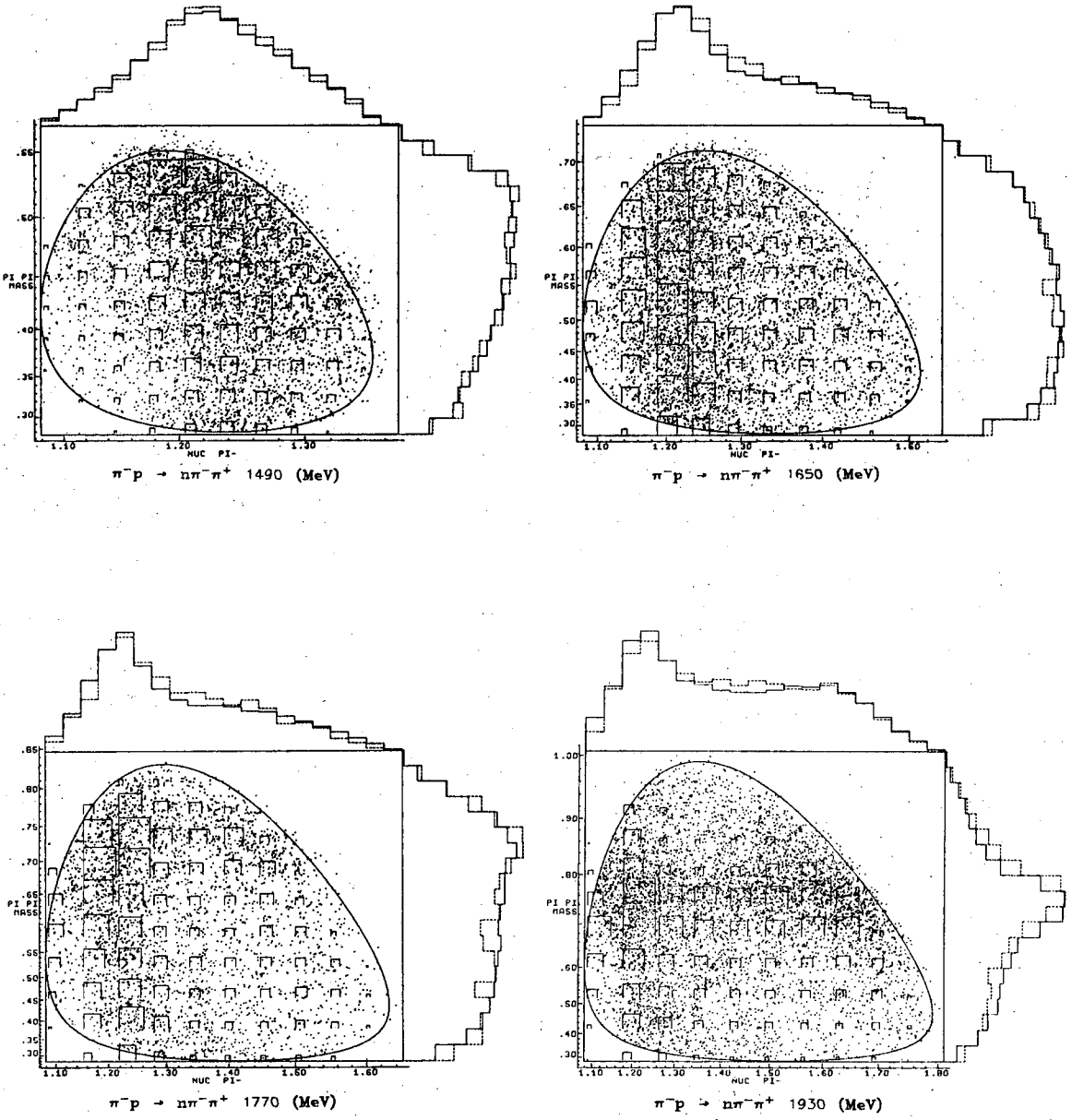

Figure 1.1

XBL 727-1289

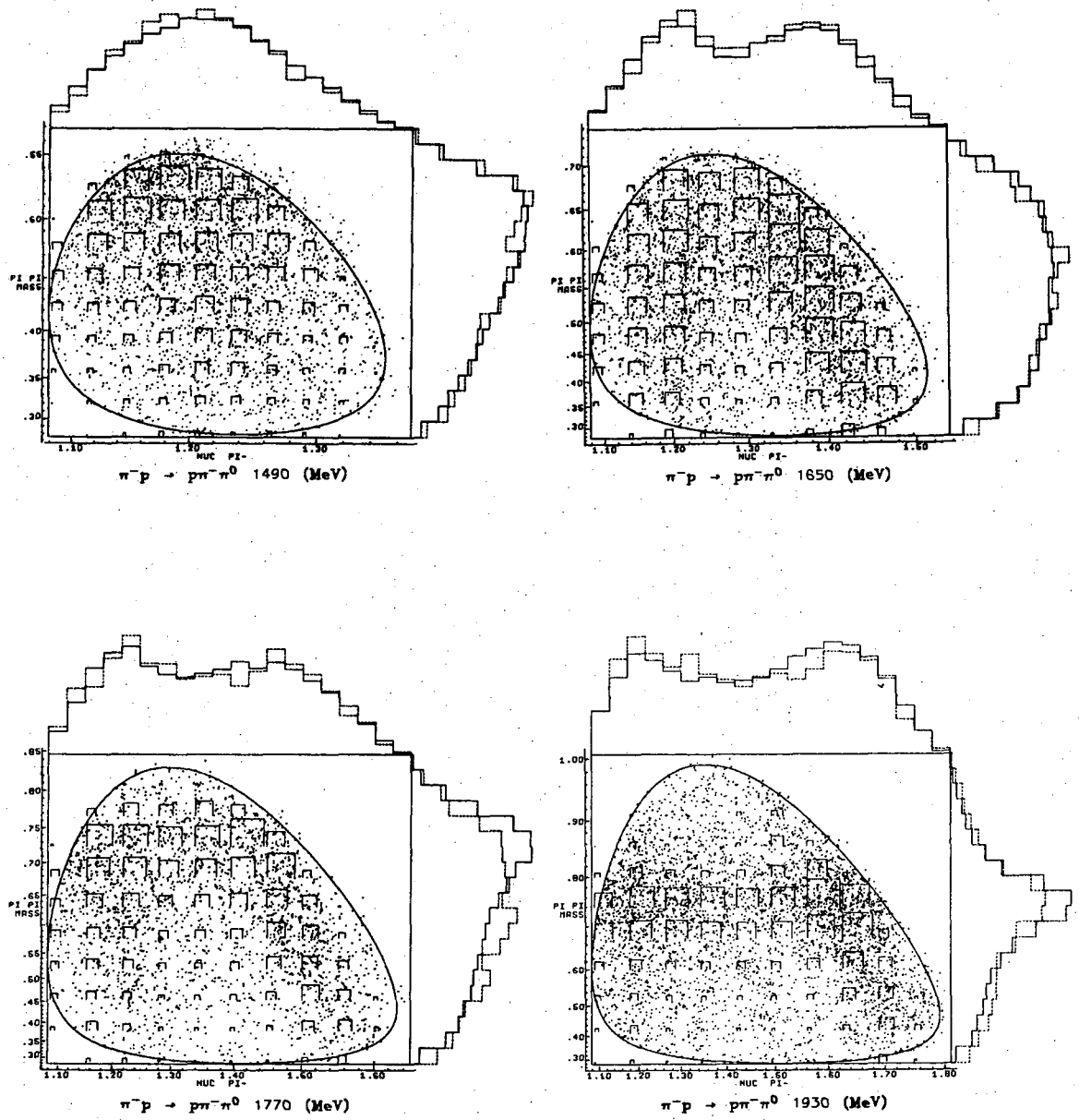

Figure 1.2

XBL 727-1290

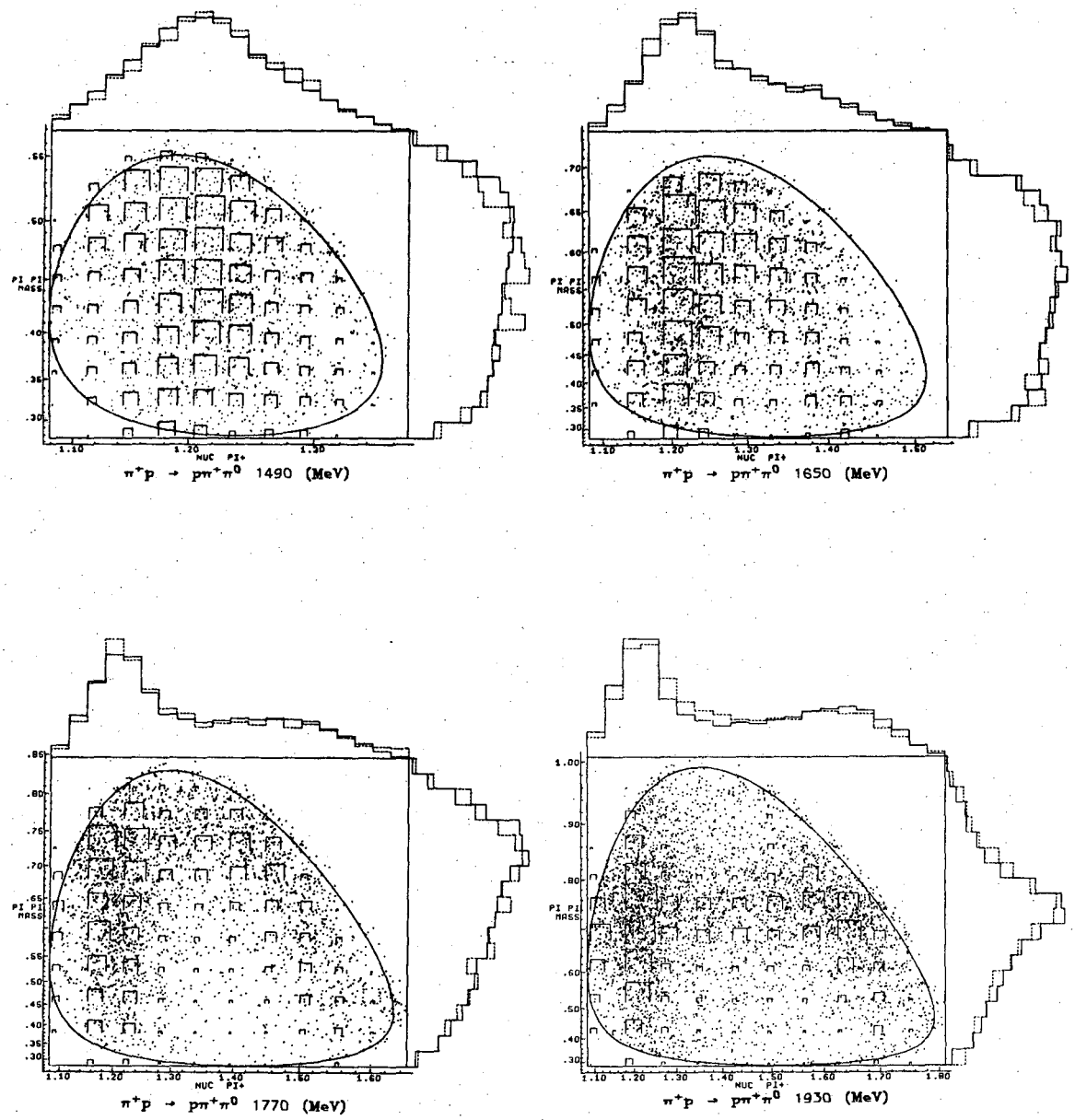

Figure 1.3

XBL 727-1291

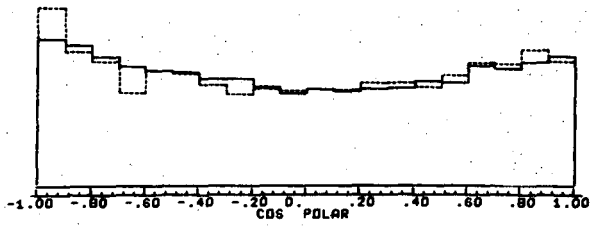

$\pi^- p \rightarrow n\pi^-\pi^+$ 1490 (MeV)

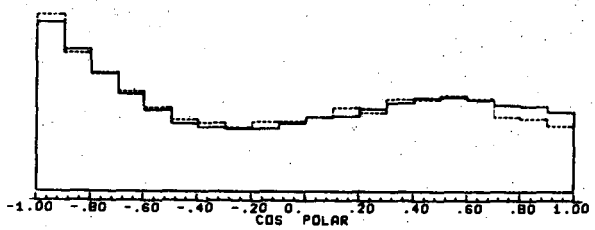

$\pi^- p \rightarrow n\pi^-\pi^+$ 1650 (MeV)

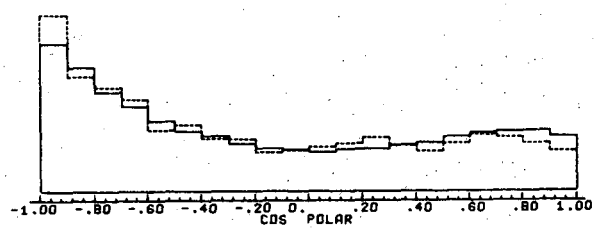

$\pi^- p \rightarrow n\pi^-\pi^+$ 1770 (MeV)

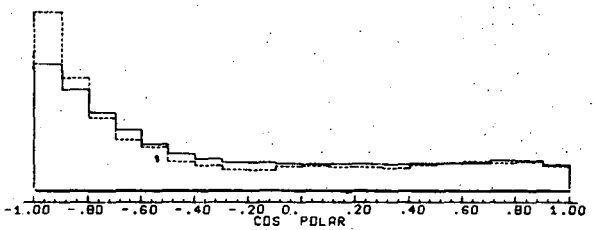

$\pi^- p \rightarrow n\pi^-\pi^+$ 1930 (MeV)

Figure 2.1

XBL 727-1292

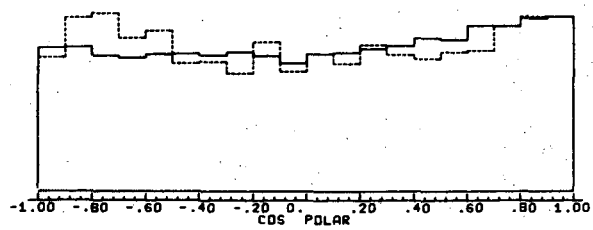

$\pi^- p \rightarrow p\pi^-\pi^0$ 1490 (MeV)

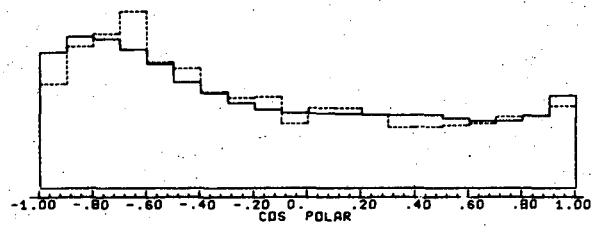

$\pi^- p \rightarrow p\pi^-\pi^0$ 1650 (MeV)

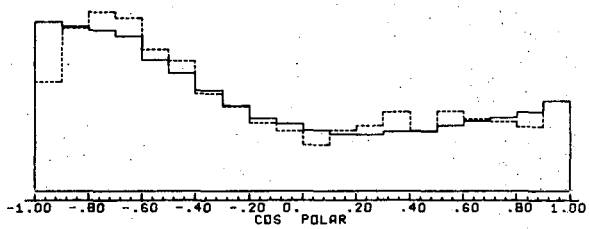

$\pi^- p \rightarrow p\pi^-\pi^0$ 1770 (MeV)

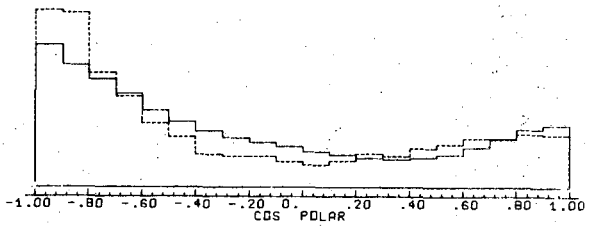

$\pi^- p \rightarrow p\pi^-\pi^0$ 1930 (MeV)

Figure 2.2

XBL 727-1293

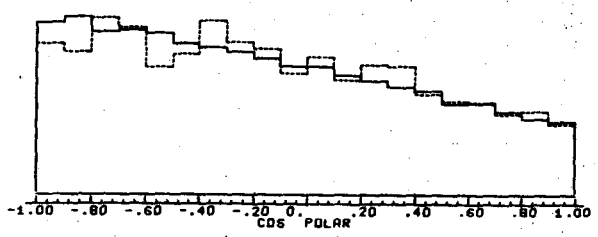

$\pi^+p \rightarrow p\pi^+\pi^0$ 1490 (MeV)

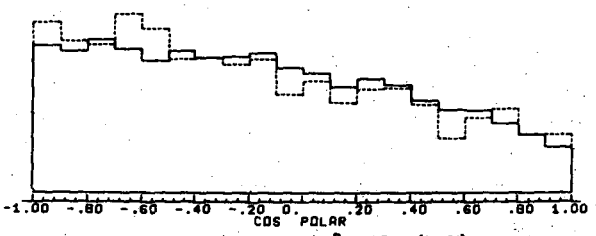

$\pi^+p \rightarrow p\pi^+\pi^0$ 1650 (MeV)

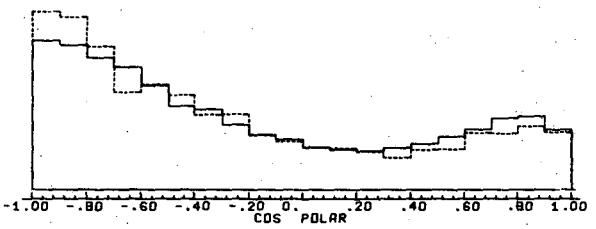

$\pi^+p \rightarrow p\pi^+\pi^0$ 1770 (MeV)

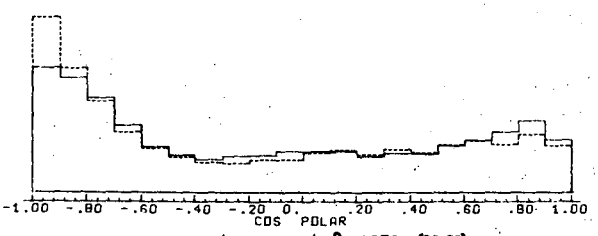

$\pi^+p \rightarrow p\pi^+\pi^0$ 1930 (MeV)

Figure 2.3

XBL 727-1294

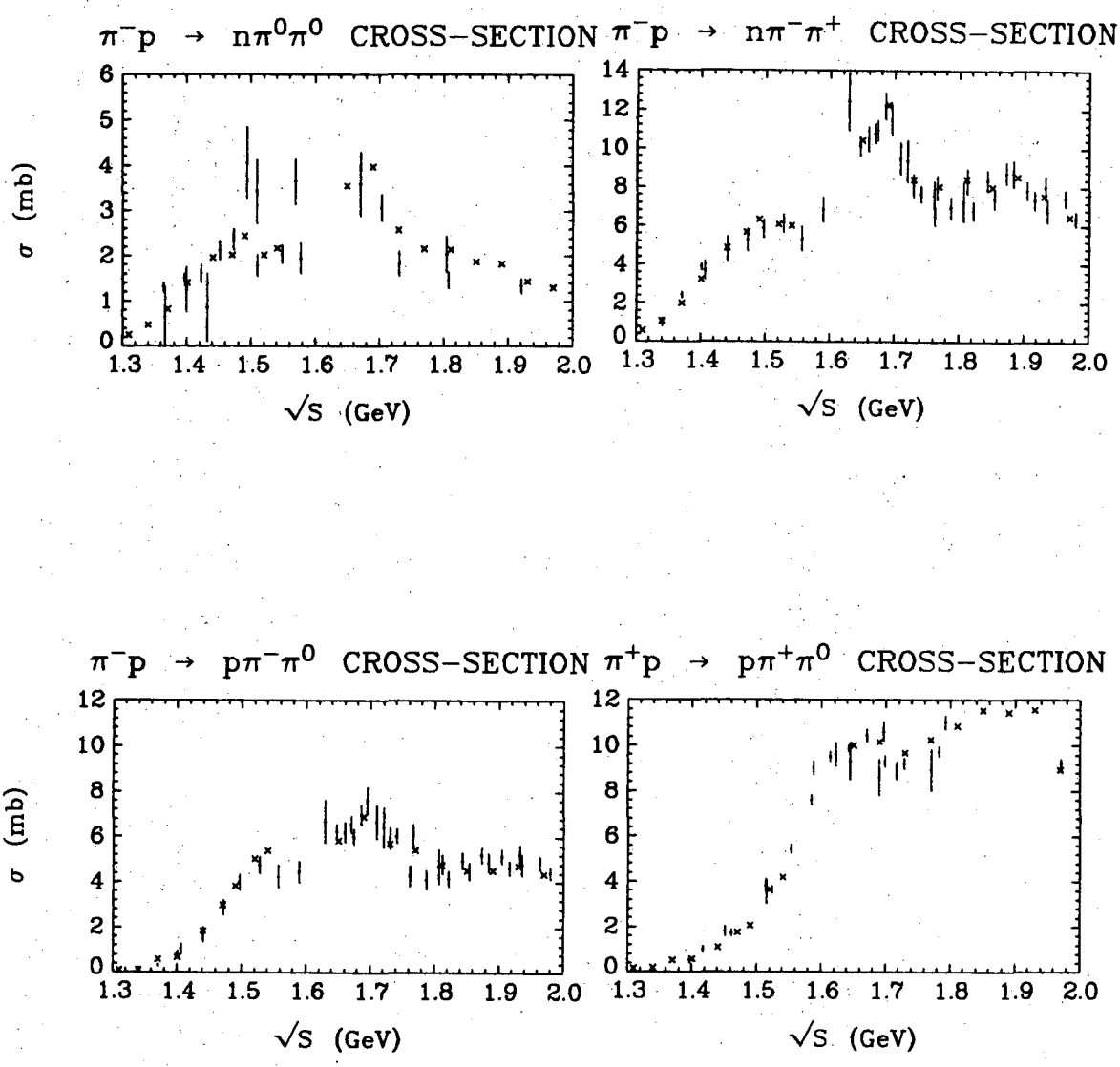

Figure 3

XBL 727-1295

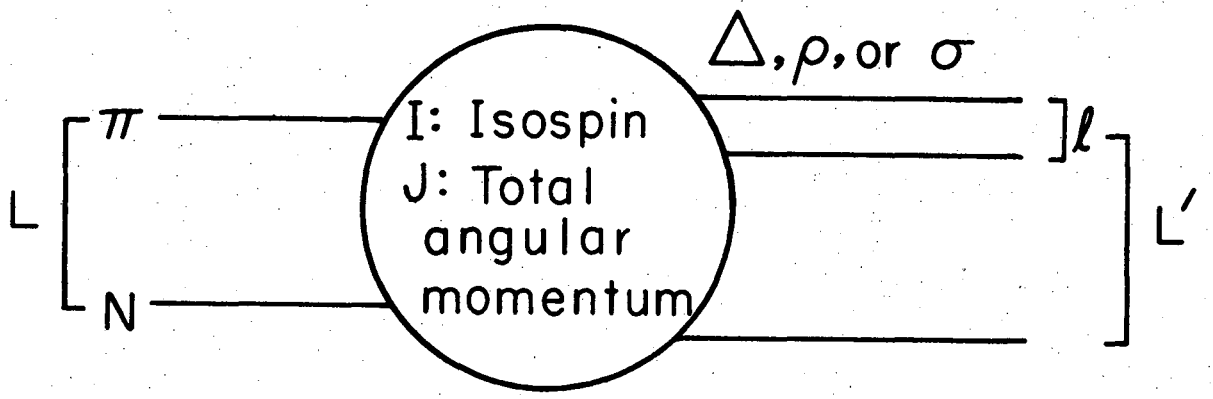

Notation for wave α: L L′ I J

Figure 4 XBL727-3454

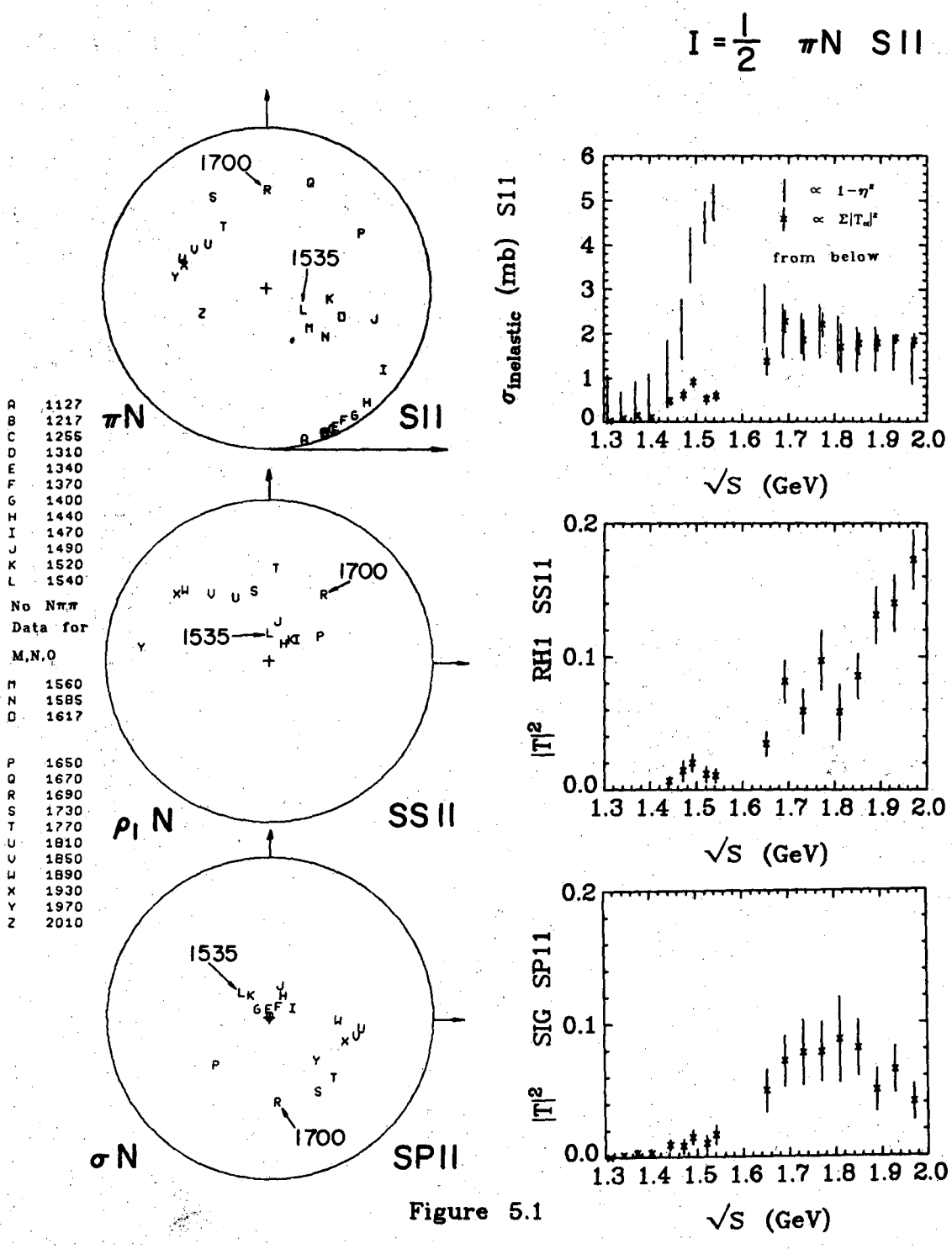

Figure 5.1

XBL 728-1512

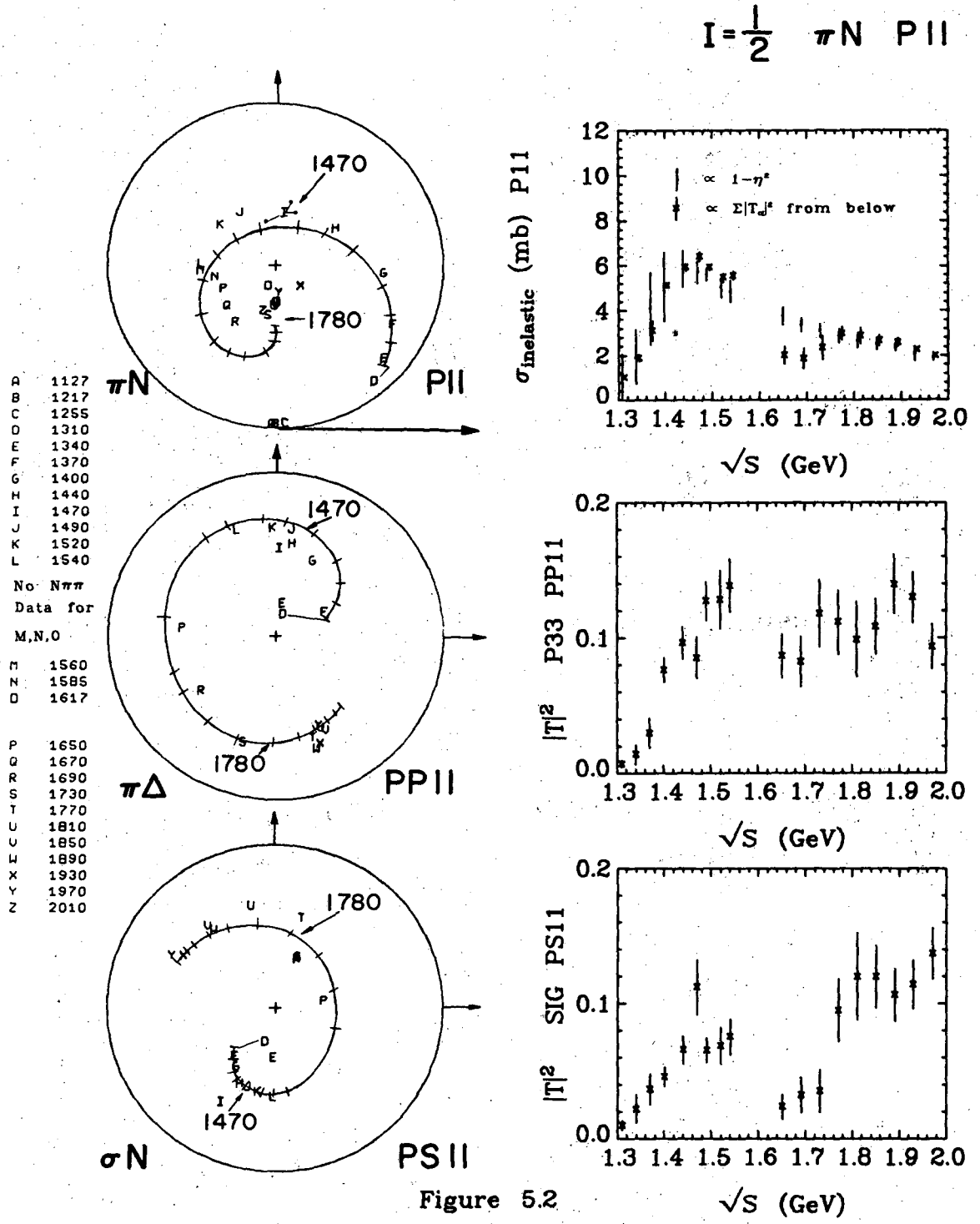

Figure 5.2

XBL 728-1513

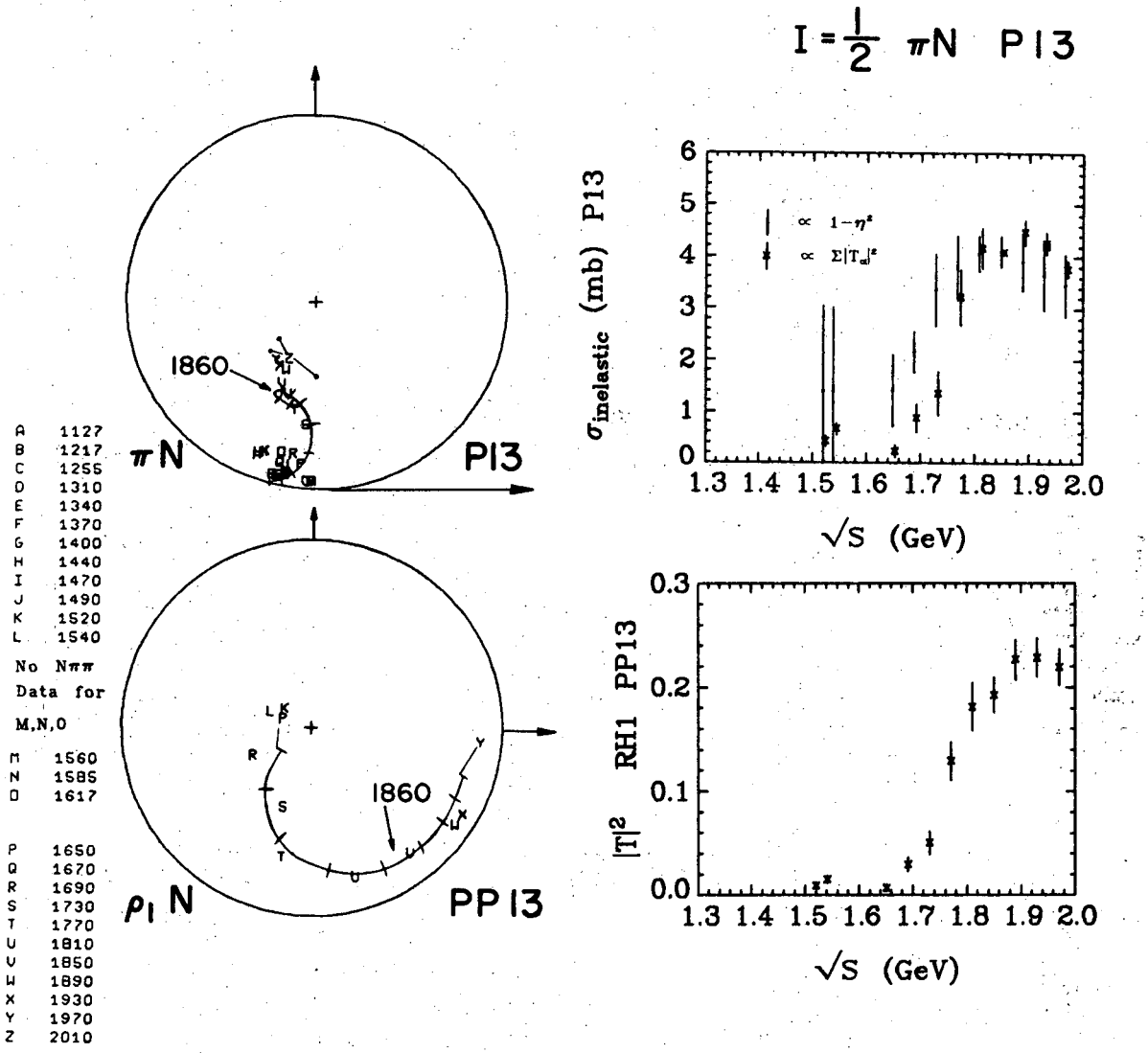

Figure 5.3

XBL 728-1514

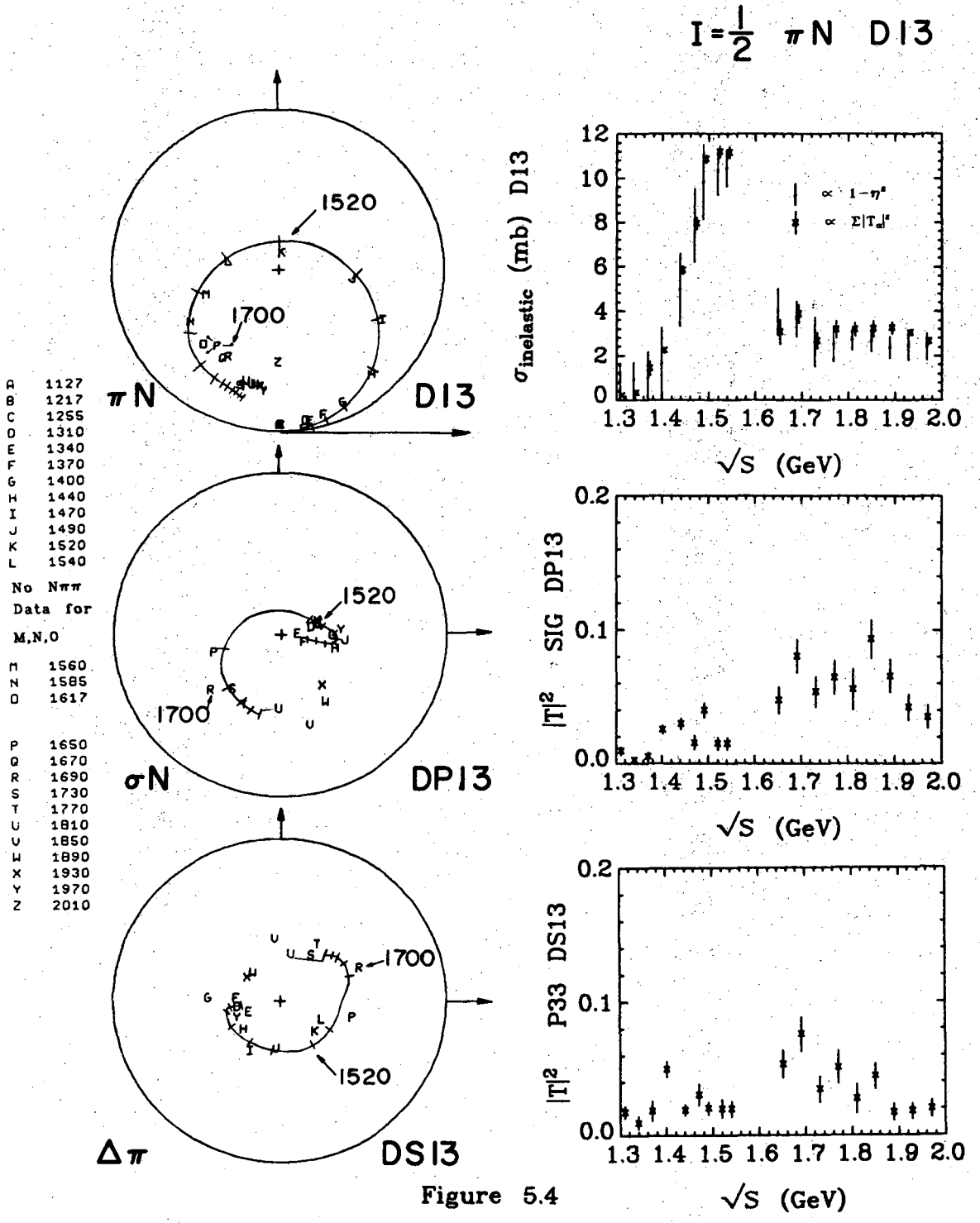

Figure 5.4

XBL 728-1515

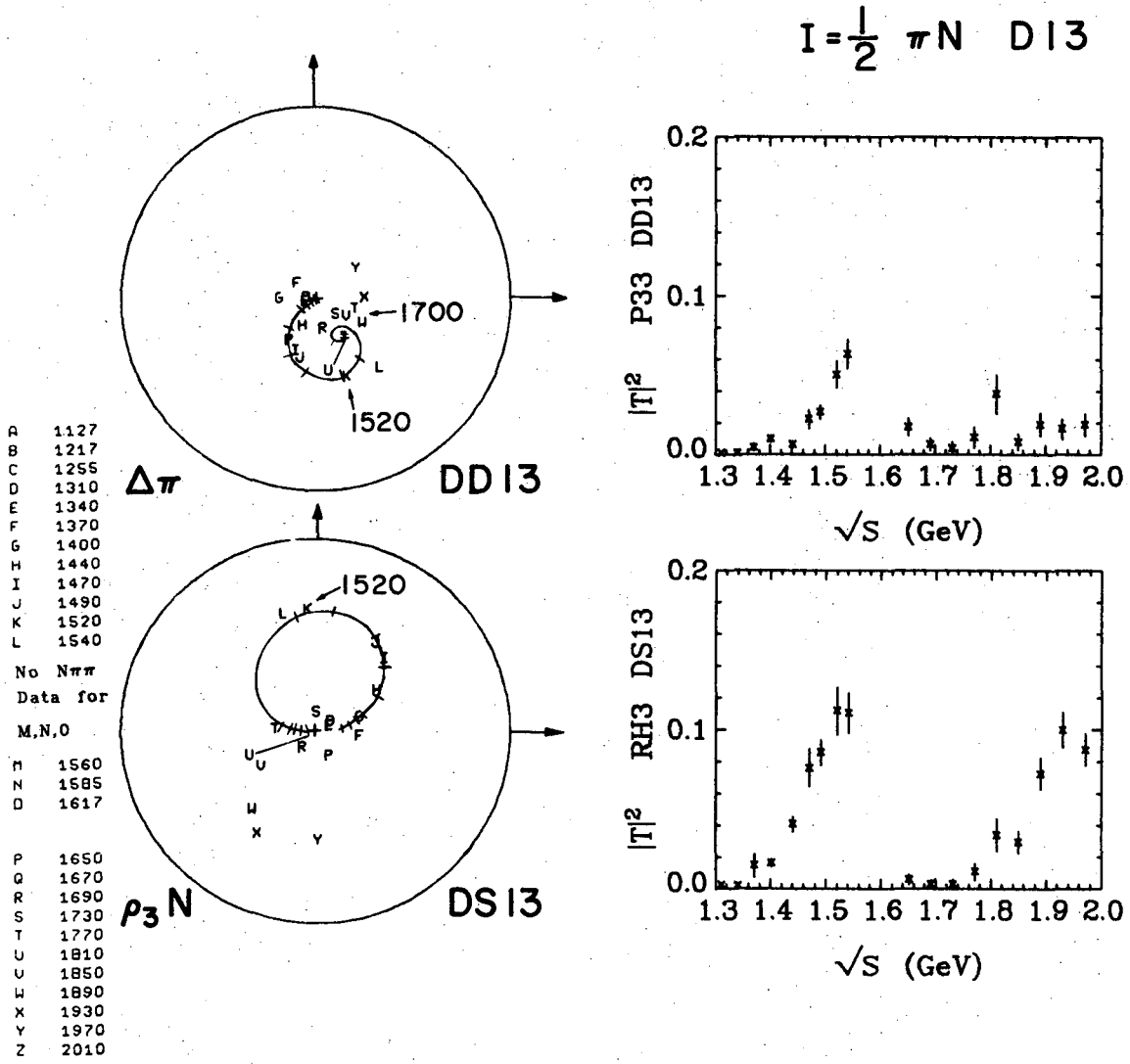

Figure 5.5

XBL 728-1516

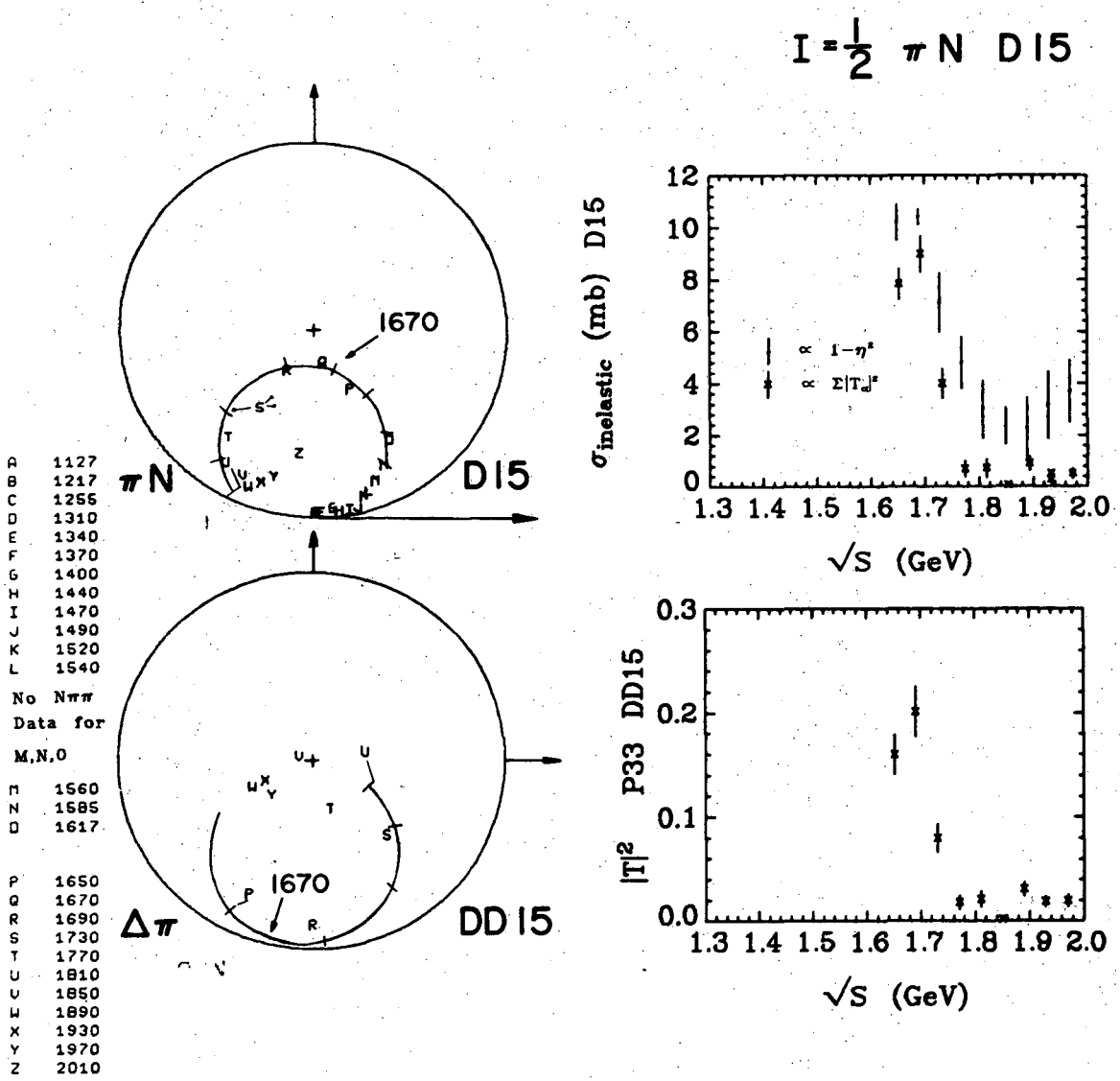

Figure 5.6

XBL 728-1517

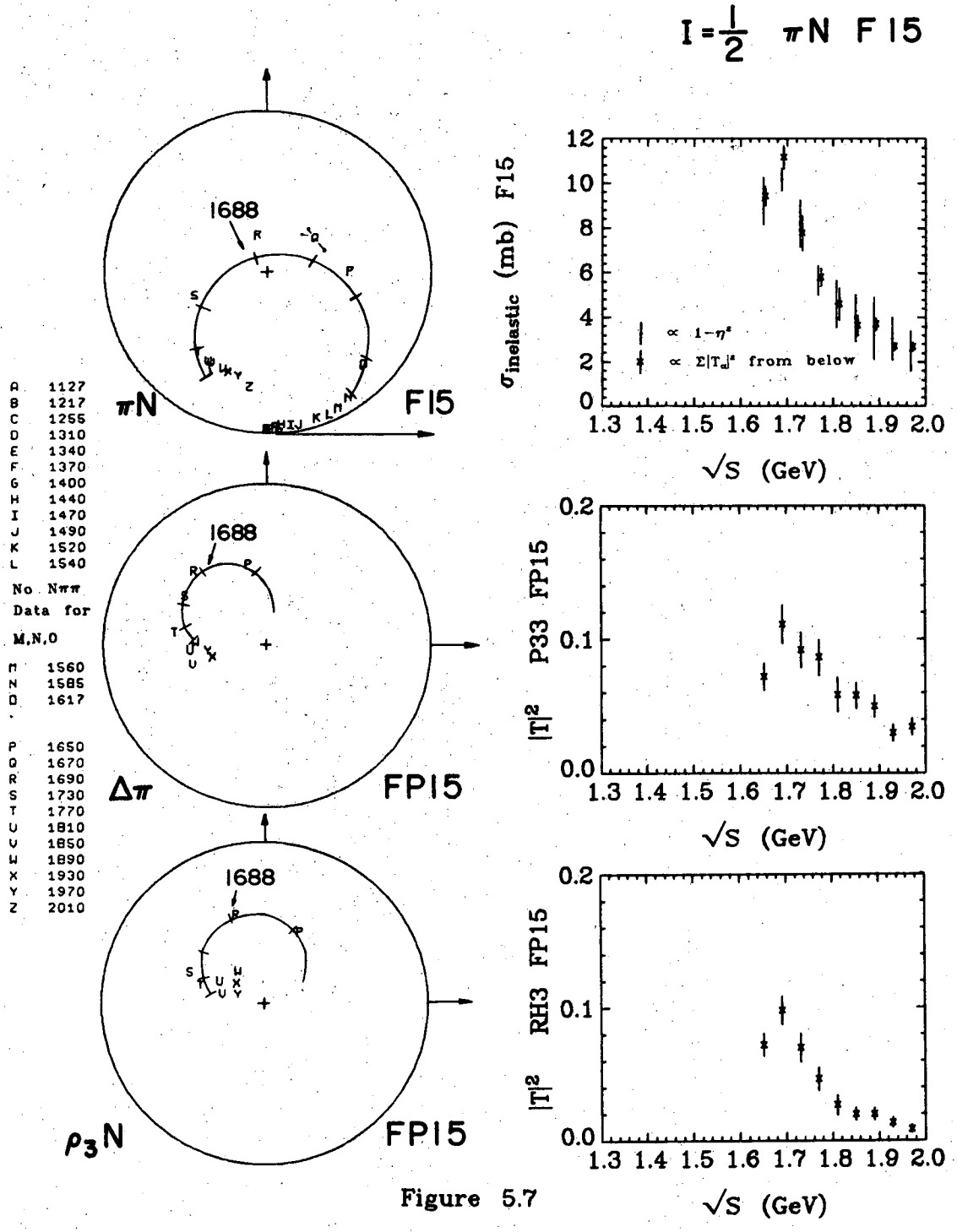

Figure 5.7

XBL 728-1518

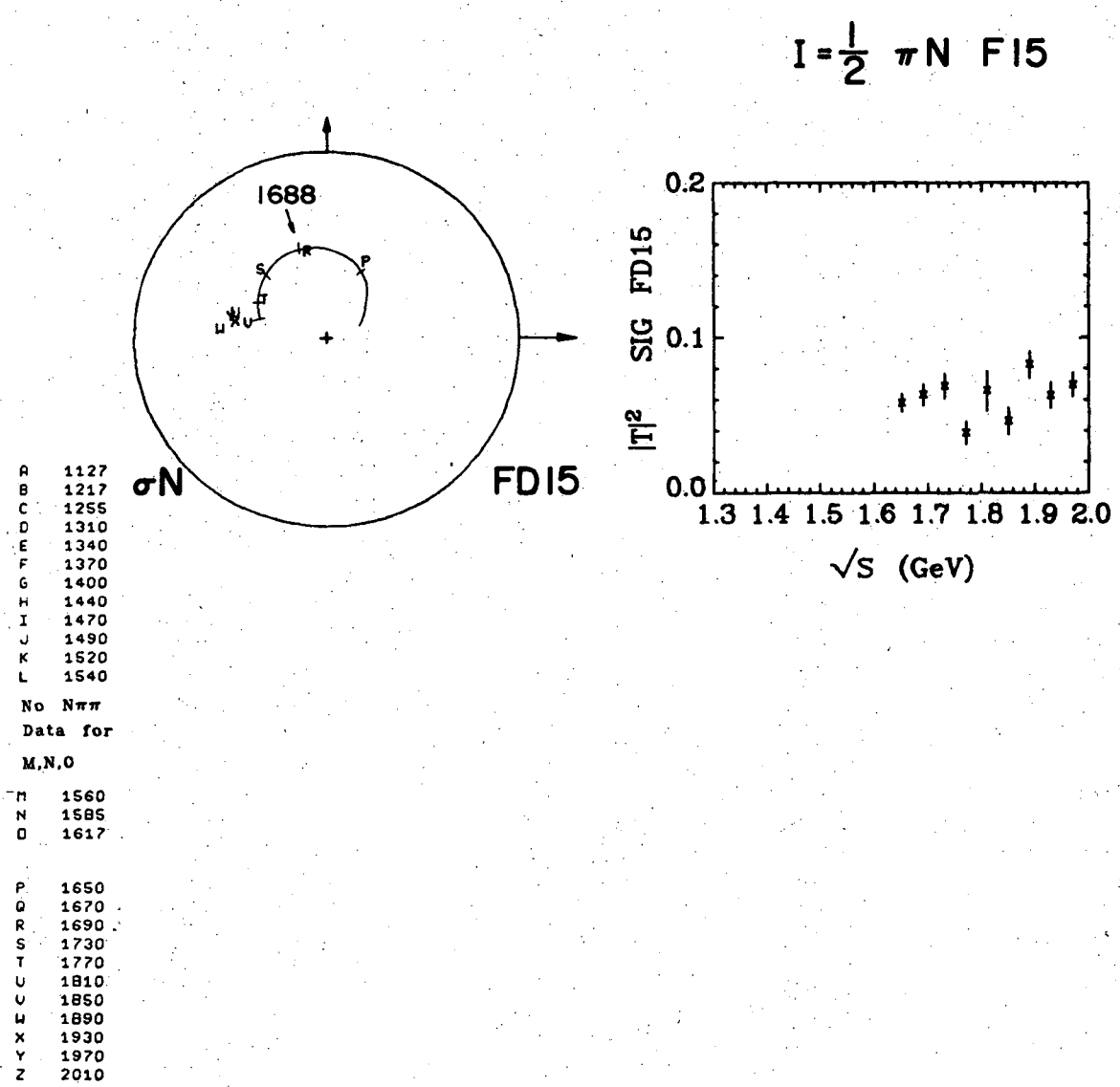

Figure 5.8

XBL 728-1519

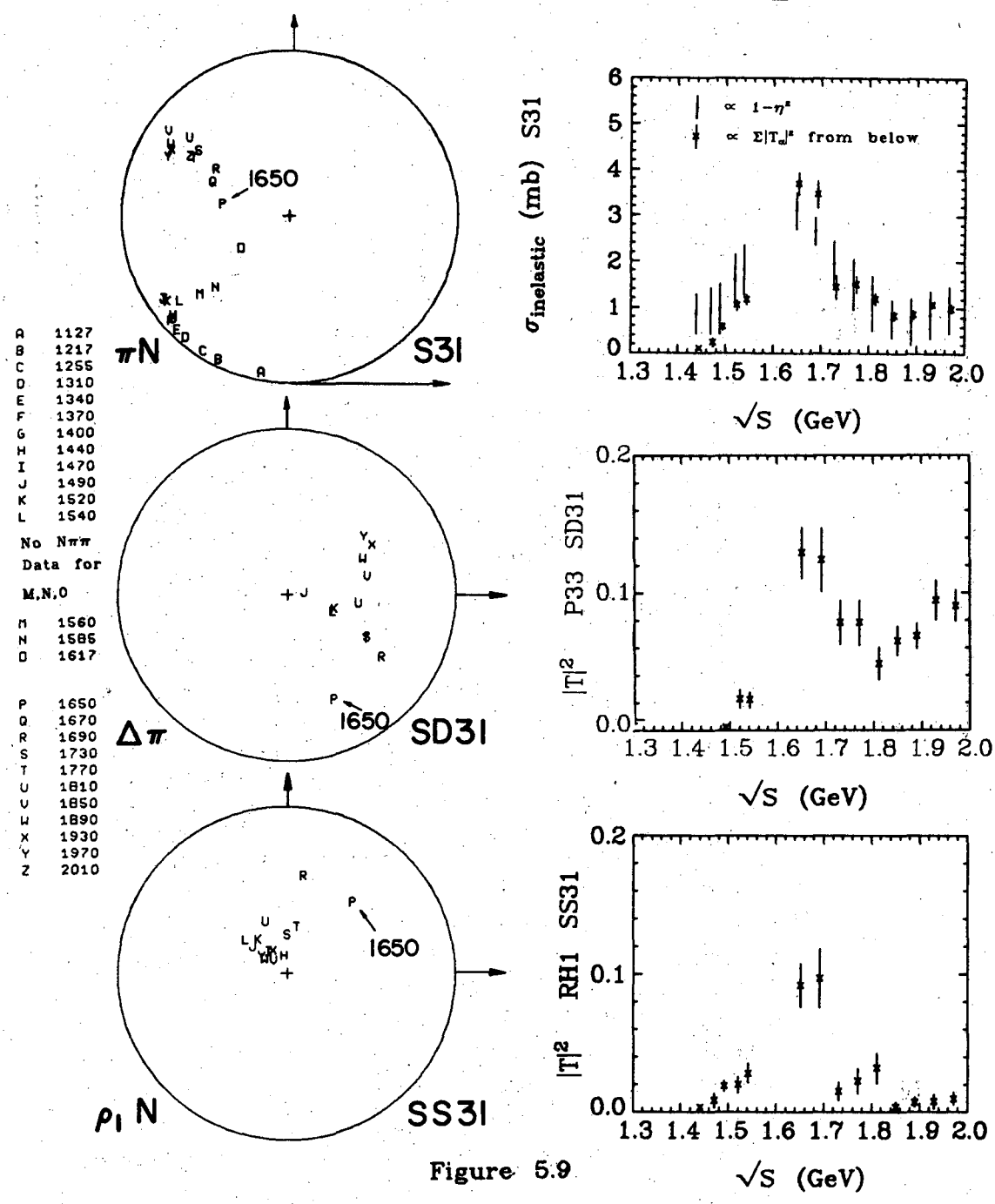

Figure 5.9

XBL 728-1520

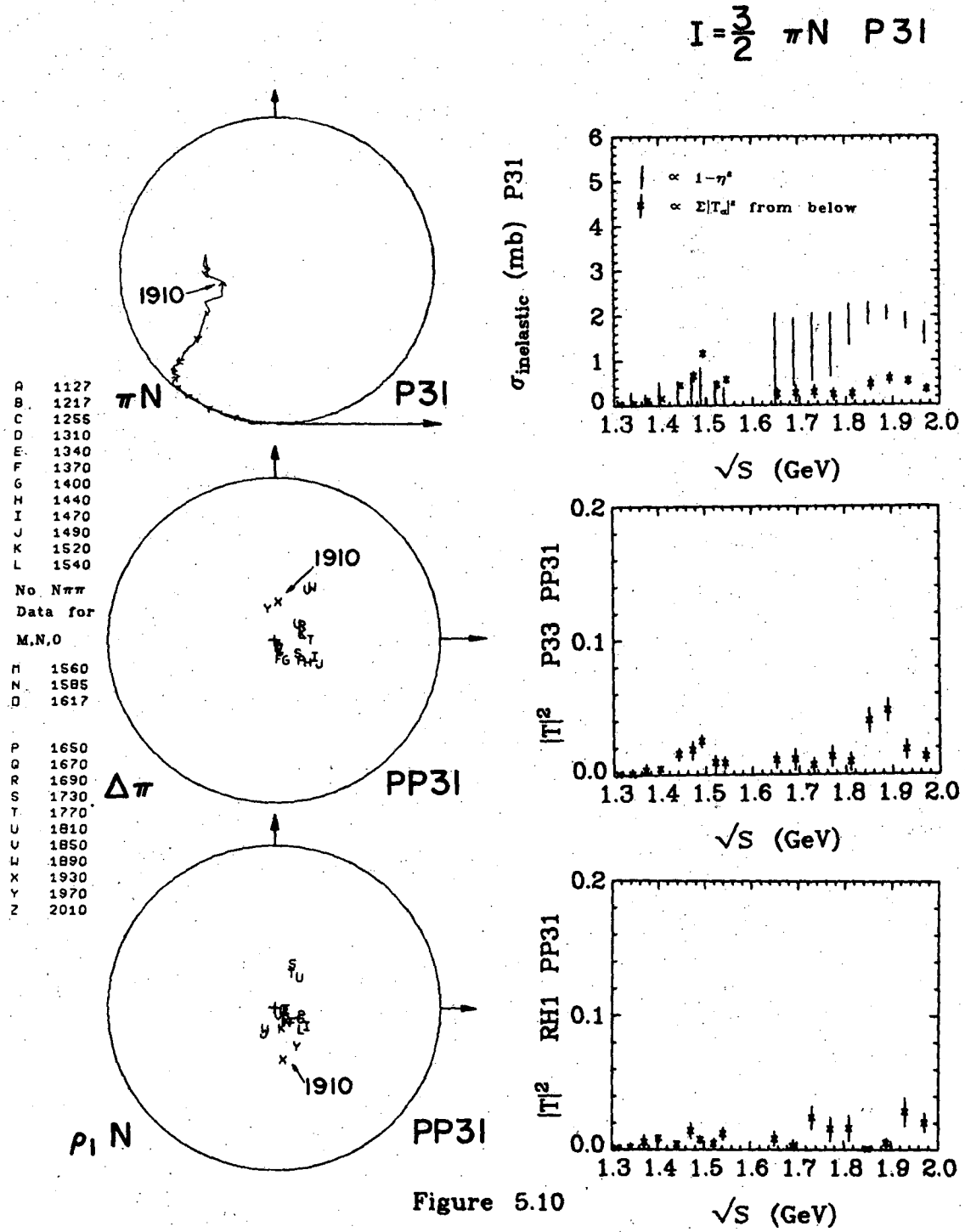

Figure 5.10

XBL 728-1521

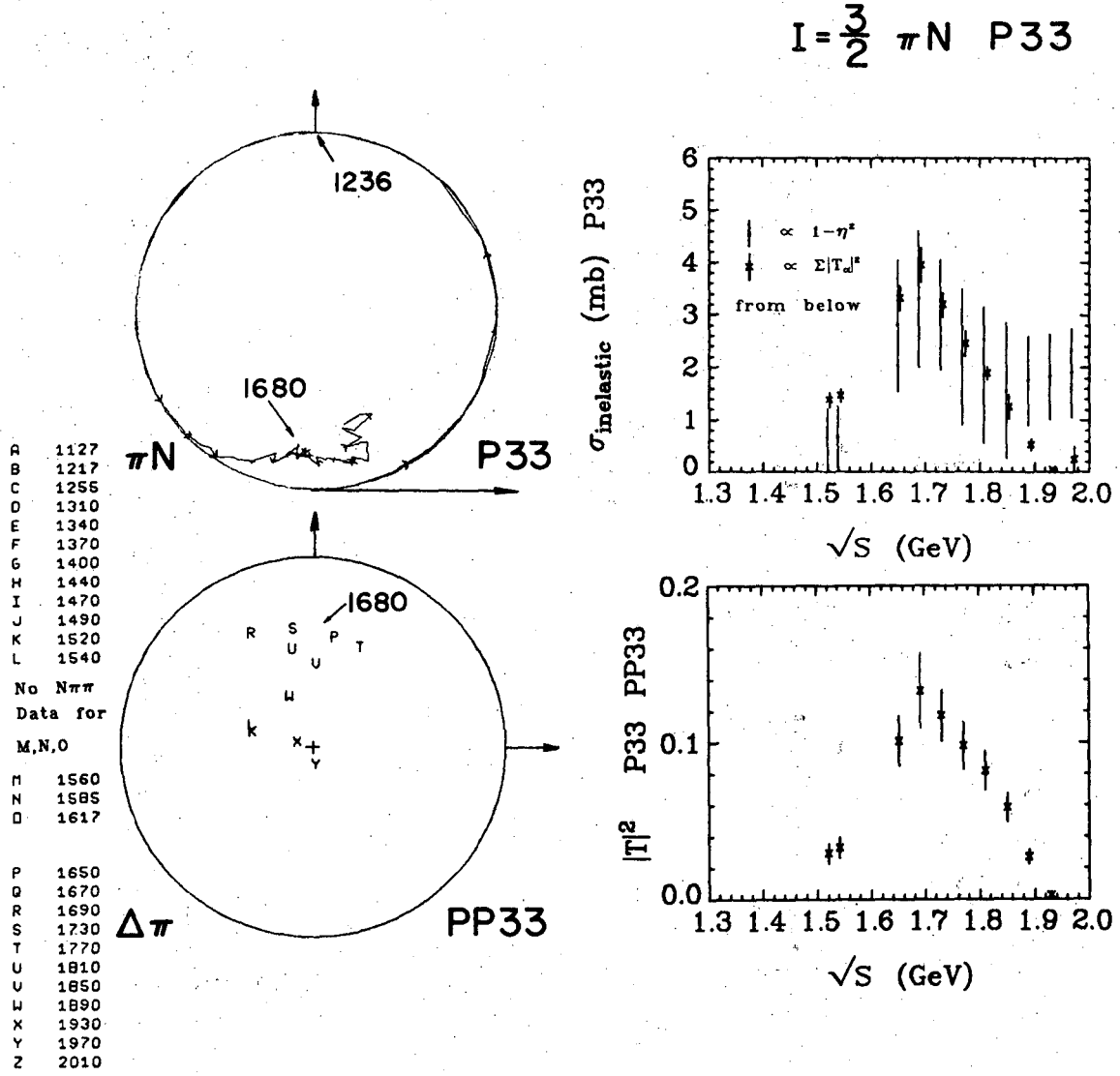

Figure 5.11

XBL 728-1522

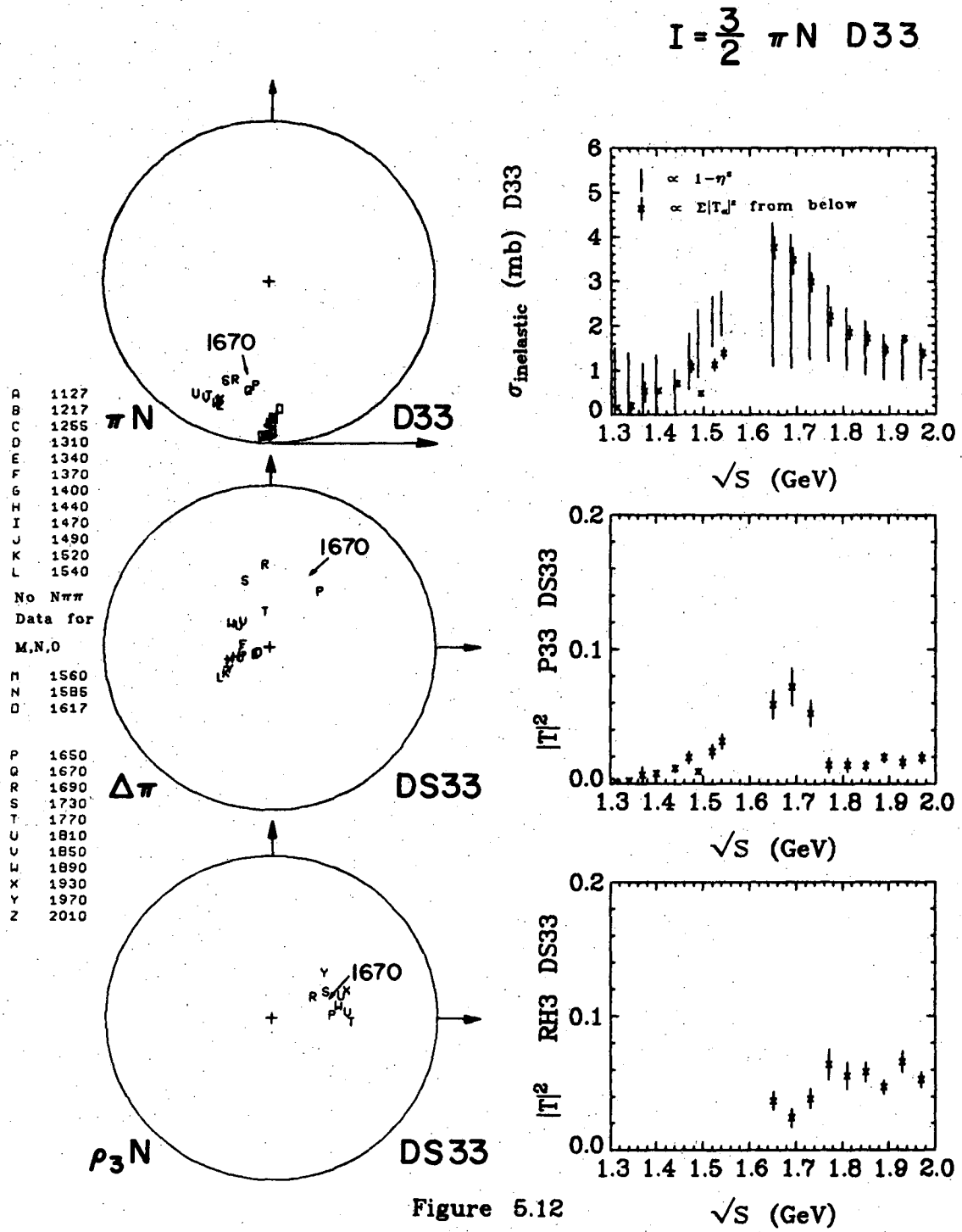

Figure 5.12

XBL 728-1523

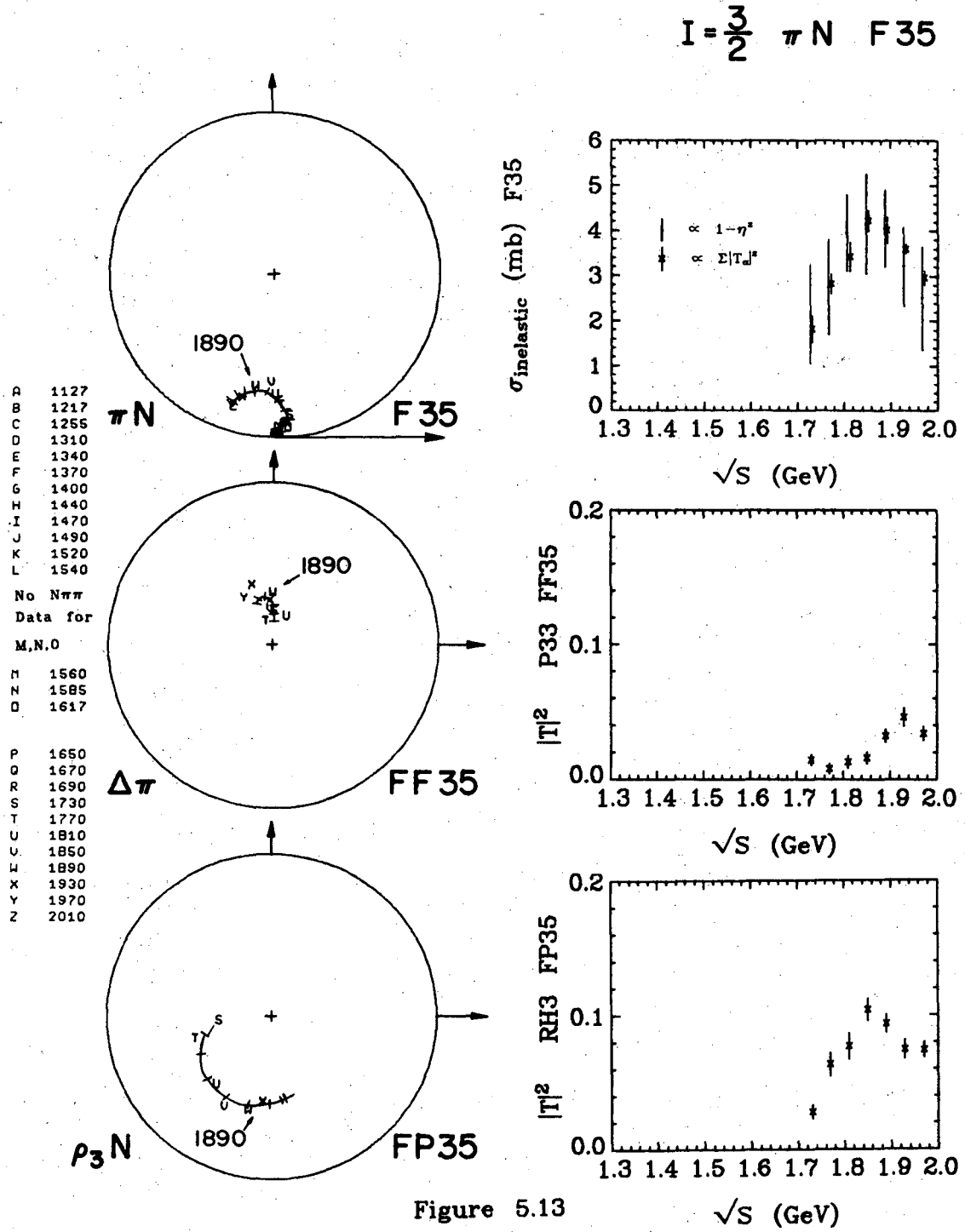

Figure 5.13

XBL 728-1524

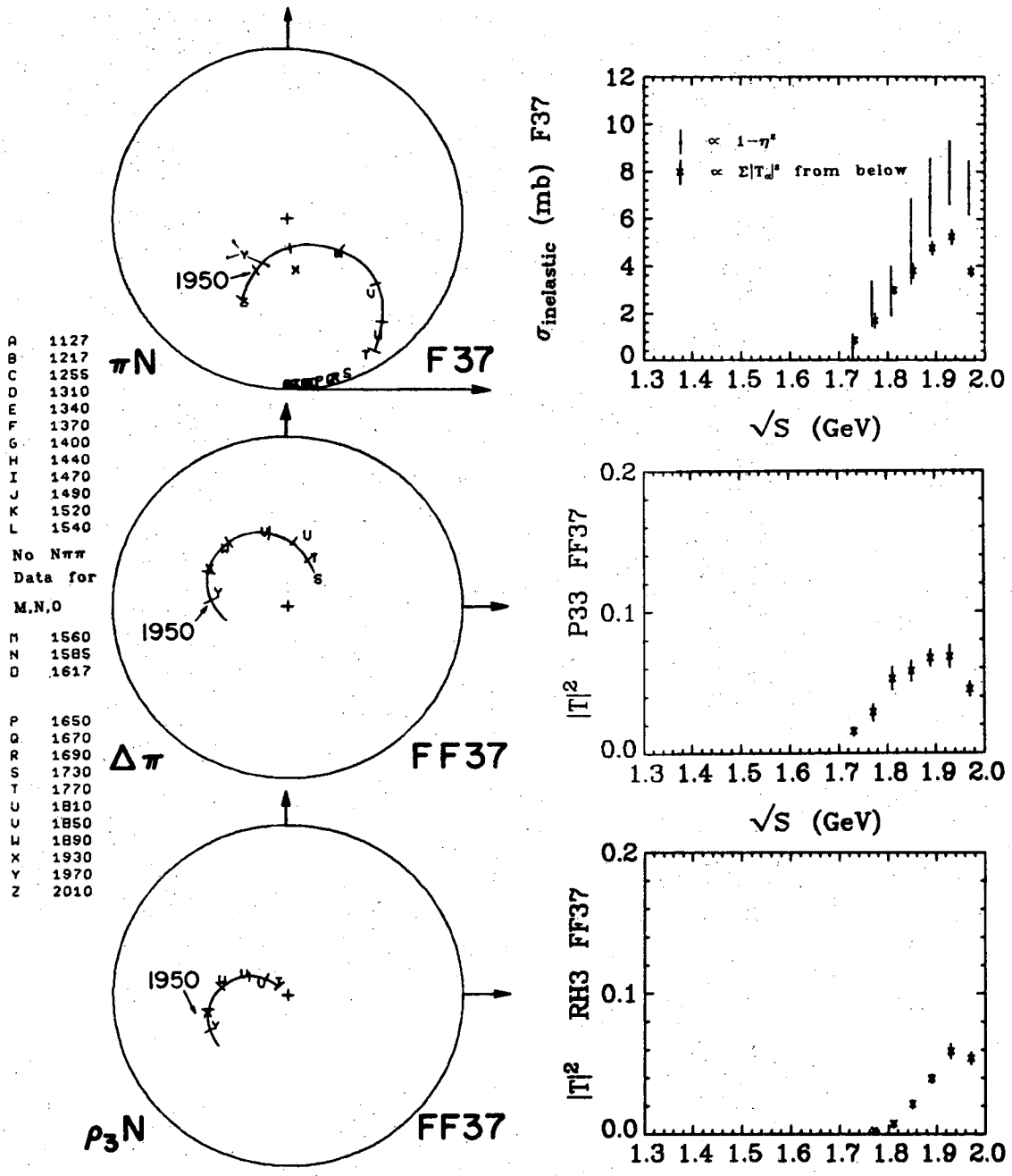

Figure 5.14

XBL 728-1525

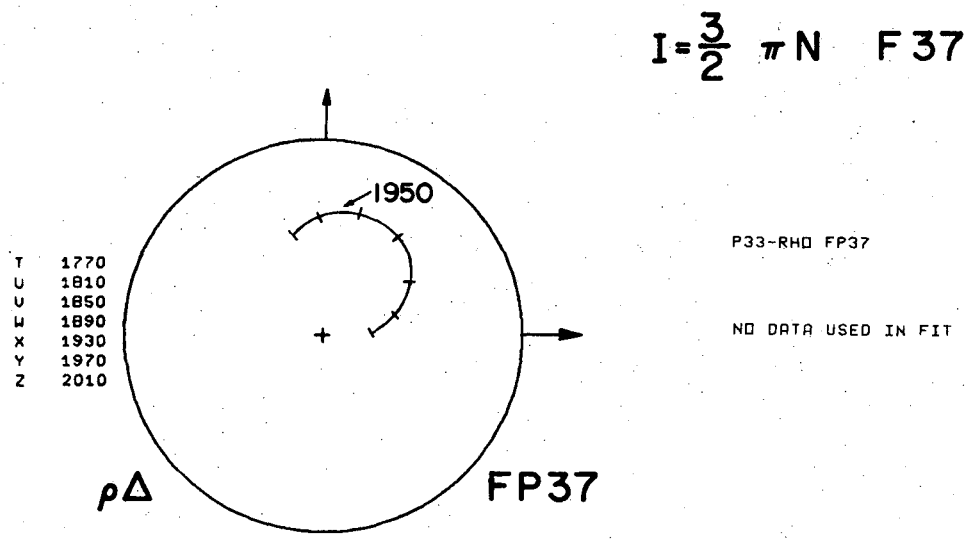

Figure 5.15

XBL 728-1526

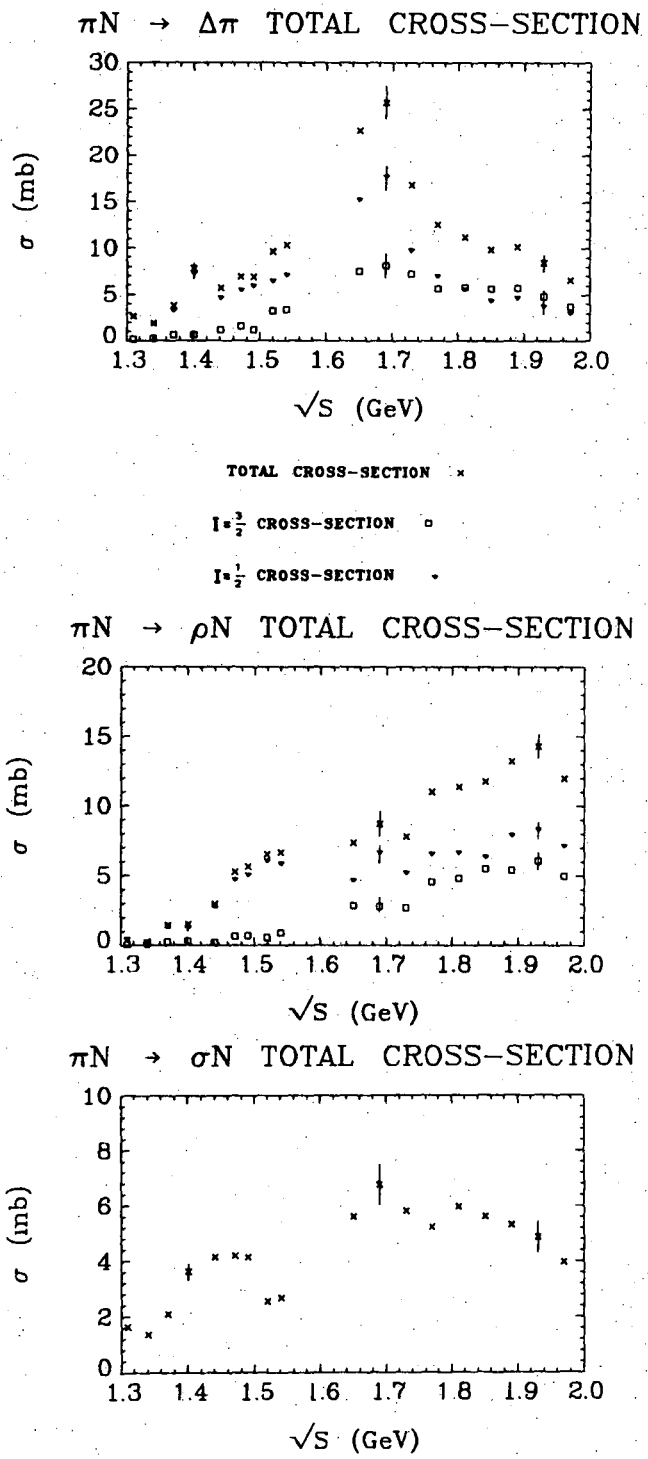

Figure 6

XBL 727-1311

TECHNICAL INFORMATION DIVISION
LAWRENCE BERKELEY LABORATORY
UNIVERSITY OF CALIFORNIA
BERKELEY, CALIFORNIA 94720